NAVAL POSTGRADUATE SCHOOL

MONTEREY, CALIFORNIA

THESIS

ASSESSMENT OF NIGHTTIME AIRBORNE VISUAL ASW CAPABILITY

by

Justin P. Goff

June 2023

Thesis Advisor: Oleg A. Yakimenko
Second Reader: Fotis A. Papoulias

Approved for public release. Distribution is unlimited.

THIS PAGE INTENTIONALLY LEFT BLANK

REPORT DOCUMENTATION PAGE	Form Approved OMB No. 0704-0188

Public reporting burden for this collection of information is estimated to average 1 hour per response, including the time for reviewing instruction, searching existing data sources, gathering and maintaining the data needed, and completing and reviewing the collection of information. Send comments regarding this burden estimate or any other aspect of this collection of information, including suggestions for reducing this burden, to Washington headquarters Services, Directorate for Information Operations and Reports, 1215 Jefferson Davis Highway, Suite 1204, Arlington, VA 22202-4302, and to the Office of Management and Budget, Paperwork Reduction Project (0704-0188) Washington, DC, 20503.

1. AGENCY USE ONLY *(Leave blank)*	2. REPORT DATE June 2023	3. REPORT TYPE AND DATES COVERED Master's thesis

4. TITLE AND SUBTITLE ASSESSMENT OF NIGHTTIME AIRBORNE VISUAL ASW CAPABILITY	5. FUNDING NUMBERS
6. AUTHOR(S) Justin P. Goff	
7. PERFORMING ORGANIZATION NAME(S) AND ADDRESS(ES) Naval Postgraduate School Monterey, CA 93943-5000	8. PERFORMING ORGANIZATION REPORT NUMBER
9. SPONSORING / MONITORING AGENCY NAME(S) AND ADDRESS(ES) N/A	10. SPONSORING / MONITORING AGENCY REPORT NUMBER

11. SUPPLEMENTARY NOTES The views expressed in this thesis are those of the author and do not reflect the official policy or position of the Department of Defense or the U.S. Government. This report contains supplemental(s).

12a. DISTRIBUTION / AVAILABILITY STATEMENT Approved for public release. Distribution is unlimited.	12b. DISTRIBUTION CODE A

13. ABSTRACT (maximum 200 words)

The United States Navy (USN) and United States Coast Guard (USCG) are shifting toward the application and use of unmanned systems to provide value to their perspective mission sets through a coordinated range of operational diversity. This research effort sought to assess the feasibility of using commercially available small Unmanned Aerial Systems (sUAS) alongside standard imaging sensors to increase the situational awareness of the maritime fleet for subsurface threats and anti-submarine warfare at night. Three lines of effort were pursued by the research team: the first two were unclassified, dealing with detection of whales, and the third line of effort was classified, processing real field data, and is included as a supplemental. The two unclassified efforts affixed commercially available imaging sensors to both manned and unmanned aircraft with the goal of detecting whales at night utilizing bioluminescence. Both fixed wing and rotary sUASs were compared as the flight platform with affixed red, green, blue (RGB) and multispectral imaging sensors. Many challenges were identified and overcome including the reduction of light pollution from the environment and aircraft, approval for sUAS beyond visual line of sight operations at night, and complications with image elongation. The final determination was that rotary sUAS systems with the MicaSense RedEdge-P was the optimal platform for capturing subsurface bioluminescent transmission at night when launched from a moving platform.

14. SUBJECT TERMS aerial, ASW, avoidance, bioluminescence, image processing, image processing toolbox, imagery, marine mammal, maritime, MATLAB, multi-spectral, semi-submersible, situational awareness, sUAS, submarine, subsurface, UAS, unmanned, warfare	15. NUMBER OF PAGES 97
	16. PRICE CODE

17. SECURITY CLASSIFICATION OF REPORT	18. SECURITY CLASSIFICATION OF THIS PAGE	19. SECURITY CLASSIFICATION OF ABSTRACT	20. LIMITATION OF ABSTRACT
Unclassified	Unclassified	Unclassified	UU

NSN 7540-01-280-5500

Standard Form 298 (Rev. 2-89)
Prescribed by ANSI Std. 239-18

THIS PAGE INTENTIONALLY LEFT BLANK

Approved for public release. Distribution is unlimited.

ASSESSMENT OF NIGHTTIME AIRBORNE VISUAL ASW CAPABILITY

Justin P. Goff
Lieutenant, United States Coast Guard
BS, North Carolina State University, 2010

Submitted in partial fulfillment of the
requirements for the degree of

MASTER OF SCIENCE IN SYSTEMS ENGINEERING

from the

NAVAL POSTGRADUATE SCHOOL
June 2023

Approved by: Oleg A. Yakimenko
Advisor

Fotis A. Papoulias
Second Reader

Oleg A. Yakimenko
Chair, Department of Systems Engineering

THIS PAGE INTENTIONALLY LEFT BLANK

ABSTRACT

The U.S. Navy (USN) and U.S. Coast Guard (USCG) are shifting toward the application and use of unmanned systems to provide value to their perspective mission sets through a coordinated range of operational diversity. This research effort sought to assess the feasibility of using commercially available small Unmanned Aerial Systems (sUAS) alongside standard imaging sensors to increase the situational awareness of the maritime fleet for subsurface threats and anti-submarine warfare at night. Three lines of effort were pursued by the research team: the first two were unclassified, dealing with detection of whales, and the third line of effort was classified, processing real field data, and is included as a supplemental. The two unclassified efforts affixed commercially available imaging sensors to both manned and unmanned aircraft with the goal of detecting whales at night utilizing bioluminescence. Both fixed wing and rotary sUASs were compared as the flight platform with affixed red, green, blue (RGB) and multispectral imaging sensors. Many challenges were identified and overcome, including the reduction of light pollution from the environment and aircraft, approval for sUAS beyond visual line of sight operations at night, and complications with image elongation. The final determination was that rotary sUAS systems with the MicaSense RedEdge-P was the optimal platform for capturing subsurface bioluminescent transmission at night when launched from a moving platform.

THIS PAGE INTENTIONALLY LEFT BLANK

TABLE OF CONTENTS

I. INTRODUCTION 1

II. MANUSCRIPT SUBMISSION 5

A. CHALLENGES IN DEVELOPING NIGHTTIME AIRBORNE MARINE MAMMAL AVOIDANCE CAPABILITY 5
B. INTRODUCTION 5
C. BACKGROUND AND LITERATURE REVIEW 6
1. Small Unmanned Aerial Systems 7
2. Bioluminescence 8
3. Current State Of COTS Light-Weight Sensor Technology 10
D. DATA COLLECTION AND PROCESSING 12
1. Test Setup 12
2. Data Processing Setup 14
E. PRELIMINARY ASSESSMENT OF SENSOR DATA 15
1. Multispectral Sensor Imagery 15
2. CMOS Sensor Imagery 17
F. CONCLUSION AND RECOMMENDATIONS 22
1. Conclusion 22
2. Recommendations for Future Work 22

III. ADDITIONAL EXPERIMENTATION AND ANALYSIS 23

A. JOINT EXPERIMENT 1: SUAS LAUNCHED FROM SHORELINE 23
1. Planning Phase 23
2. Data Collection 28
3. Data Analysis 30
B. LABORATORY TESTING OF SENSORS 38
C. JOINT EXPERIMENT 2: SUAS LAUNCHED FROM OFFSHORE VESSEL 44
1. Planning Phase 44
2. Data Collection 46
3. Data Analysis 48

IV. CONCLUSION 53

A. CONCLUSION 53
1. Flight System 53

2. Sensor Systems 54
B. FUTURE WORK 55

APPENDIX. MATLAB CODE 57
A. CALCULATE AND GRAPH IMAGE INTENSITY 57
B. PROCESS MICASENSE REDEDGE-MX TIFF IMAGE FILES 58
C. ADJUST IMAGE INTENSITY SATURATION 60
D. PROCESS MICASENSE REDEDGE-P TIFF IMAGE FILES 61
E. MP4 VIDEO PROCESSING 64

SUPPLEMENTALS 67
A. SUPPLEMENTAL 1: PRESENTATION OF HOODTECH RESEARCH RESULTS 67
B. SUPPLEMENTAL 2: CLASSIFIED ANALYSIS OF ASW SUMMARY BRIEF VIDEO FILES. THIS ANALYSIS IS CLASSIFIED SECRET. 67
C. SUPPLEMENTAL 3: PRESENTATION OF NON-ACOUSTIC ASW OVERVIEW. THIS PRESENTATION IS CLASSIFIED SECRET//NOFORN. 67
D. SUPPLEMENTAL 4: VIDEO SUMMARY OF ASW EXERCISE RESULTS AND BIOLUMINESCENCE RESEARCH. THIS VIDEO IS CLASSIFIED SECRET. 67

LIST OF REFERENCES 69

INITIAL DISTRIBUTION LIST 73

LIST OF FIGURES

Figure 1. Growth of worldwide naval and merchant vessel fleet reported by the IMO since 1980. Adapted from [1]. 1

Figure 2. Humpback whales struck by a merchant vessel can be carried far from the impact site. Source: [3]. 2

Figure 3. USCG Cutter Munro (WMSL-755) crew members inspect a self-propelled semi-submersible on June 19, 2019, in international waters of the Eastern Pacific Ocean. Source: [5]. 3

Figure 4. Tracker data from merchant vessels and whales in northern Chilean Patagonia. Adapted from [7]. 6

Figure 5. A 1974 image of fish escaping from a trawler's net off the California coast. Source: [8]. 7

Figure 6. Visual enhancement of captured electro-optical imagery of a humpback whale in Monterey Bay, CA. Source: [10]. 8

Figure 7. Dinoflagellates illuminate shorelines waves off the coast of Big Sur near Monterey Bay, California. Source: [12]. 9

Figure 8. MicaSense 10-band dual camera system (a), and combined Sony UMC-R10C and 5-band MicaSense RedEdge-MX (b). Source: [13]. 10

Figure 9. SBIG STC-428-OEM scientific CMOS imaging camera. Source: [16]. 11

Figure 10. CMOS imaging camera assembly mounted within a custom 3-D enclosure. Source: [10]. 12

Figure 11. Quantum Systems Trinity F90+ eVTOL sUAS equipped with multispectral sensor. Source: [10]. 13

Figure 12. General aviation aircraft with affixed image capturing platform equipped with the low-light SBIG CMOS-based sensor. Source: [10]. 14

Figure 13. Footprint per pixel for MicaSense RedEdge-MX sensor flown on a sUAS. Source: [10]. 15

Figure 14. Image shift for a low-flying fixed wing sUAS cruising at 17m/s. Source: [10]. 16

Figure 15. The Blue-band grayscale image of a humpback whale in Monterey Bay captured with MicaSense RedEdge-MX from a low-flying sUAS with enhanced contrast using histogram equalization. Source: [10]. 17

Figure 16. Footprint per pixel for low-light sensor flown on a general aviation aircraft. Source: [10]. 18

Figure 17. Image shift for CMOS sensor mounted on a general aviation aircraft flying at a typical cruise speed. Source: [10]. 18

Figure 18. Image with a 0.07s exposure when flying at 1,200m (4,000ft) MSL at 40m/s (77kts). Source: [10]. 19

Figure 19. Monterey Bay, California Fisherman's Wharf in daylight, (a), and the nighttime illumination of the same object, (b), with 0.7s exposure at 1,200m MSL and speed of 40m/s. Source: [10]. 19

Figure 20. Artistic representation of the effect of elongated exposure time (true to scale). Source: [10]. 20

Figure 21. The 70s exposure images taken with (a) and without (b) bioluminescence filter. Source: [10]. 21

Figure 22. Visualization of the member agency logos who partnered during the September 27, 2022, experimentation. Adapted from [21]–[28]. 23

Figure 23. MBARI Dorado class AUV used in Joint Experiment 1. Source: [29]. 24

Figure 24. Average bioluminescent potential for Monterey Bay, CA based on latitude and time of year. Adapted from [30]. 25

Figure 25. Heatmap of bioluminescent intensity for Monterey Bay with sUAS launch location, USCG small boat pier, and AUV track line. Adapted from [30]. 26

Figure 26. Operational Concept (OV-1) for the September 27, 2022, Joint Experiment 1. 27

Figure 27. USCG MLB from Station Monterey, CA. Source: [32]. 27

Figure 28. Trinity F90+ flight 1 information. 28

Figure 29. Trinity F90+ flight 2 information. 29

Figure 30. Maximum, minimum, and average change in intensity, normalized, for the blue band centered on 475nm from the MicaSense RedEdge-MX for Mission 1 31

Figure 31. Analysis of Mission 1 images from the MicaSense RedEdge-MX plotting each individual sensors image intensity on a normalized scale from 0 to 1 32

Figure 32. Maximum, minimum, and average change in intensity, normalized, for RGB images captured using the Sony UMC-R10C for Mission 2. 33

Figure 33. Analysis of Mission 2 images from the MicaSense RedEdge-MX plotting each individual sensors image intensity on a normalized scale from 0 to 1 35

Figure 34. RGB image from the Sony UMC-R10C during Mission 2 alongside five individual bands captured by the MicaSense Red-Edge MX at the same timestamp. 36

Figure 35. Sony UMC-R10C images processed to show individual color channels fraction of intensity per frame for Mission 2. 37

Figure 36. Trinity F90+ sUAS with affixed anticollision lighting prior to launch. 37

Figure 37. Trinity F90+ payload compartment while powered on showing light pollution from internal blue light and red light on payload. 38

Figure 38. Quantum Systems payload with Sony RXR1-RII payload. Source: [13]. 39

Figure 39. Image sensor testing setup. 40

Figure 40. Gray scale blue band image from the MicaSense RedEdge-MX (a) and the RGB image from the Sony UMC-R10C (b) 41

Figure 41. Test image from the Sony UMC-R10C split into three individual, RGB color channels. 42

Figure 42. Analysis of image intensity change for each sensor as light intensity was increased incrementally. 43

Figure 43. Monterey Bay Whale Watch vessel Pt. Sur Clipper. Source: [27]. 44

Figure 44. DJI Matrice 300 RTK rotary sUAS flown by NOAA. Source: [33]. 45

Figure 45. MicaSense RedEdge-P multispectral sensor plus panchromatic. Source: [34]. 46

Figure 46. Vessel track line during the March 30, 2023, Joint Experiment 2. 47

Figure 47. Team member launching sUAS from the stern of the Pt. Sur Clipper during the March 30, 2023, Joint Experiment 2. 47

Figure 48. Maximum, minimum, and average change in intensity, normalized, for the blue band centered on 475nm from the MicaSense RedEdge-P during Joint Experiment 2. 48

Figure 49. Blue band image before (a) and after (b) adjustment of intensity saturation. 49

Figure 50. Maximum, minimum, and average change in intensity, normalized, for panchromatic images from the MicaSense RedEdge-P during Joint Experiment 2. 50

Figure 51. Panchromatic image before (a) and after (b) adjustment of intensity saturation. 51

Figure 52. Analysis of all images during Joint Experiment 2 from the MicaSense RedEdge-P plotting each individual sensors image intensity on a normalized scale from 0–1. 52

LIST OF TABLES

Table 1. Trinity F90+ sUAS sensor specifications. Adapted from [13]. 39

THIS PAGE INTENTIONALLY LEFT BLANK

LIST OF ACRONYMS AND ABBREVIATIONS

3-D	Three-Dimensional
AIS	Automatic Identification System
ASW	Anti-Submarine Warfare
AUV	Autonomous Underwater Vehicle
BVLOS	Beyond Visual Line of Sight
CMOS	Complementary Metal-Oxide Semiconductor
COA	Certificate of Authorization
COTS	Commercial-Off-The-Shelf
DMO	Distributed Maritime Operations
eVTOL	Electric Vertical Take-Off and Landing
FAA	Federal Aviation Administration
IMO	International Maritime Organization
IWC	International Whaling Convention
MBA	Monterey Bay Academy
MBARI	Monterey Bay Aquarium Research Institute
MLB	47-foot Motor Lifeboat
MP	Megapixels
MSL	Mean Sea Level
NOAA	National Oceanic and Atmospheric Administration
NPS	Naval Postgraduate School
OV-1	Operational Concept Diagram
RGB	Red, Green, Blue
SD	Secure Digital
sUAS	Small Unmanned Aerial Systems
USCG	United States Coast Guard
USN	United States Navy

THIS PAGE INTENTIONALLY LEFT BLANK

EXECUTIVE SUMMARY

The United States Navy (USN) and United States Coast Guard (USCG) are shifting toward the application and use of unmanned systems to provide value to their perspective mission sets through a coordinated range of operational diversity. The Distributed Maritime Operations concept outlines the need for integration of these non-traditional assets into the USN and USCG strategic decision processes. This research effort desires to assess the feasibility of using commercially available unmanned aircraft alongside standard imaging sensors to increase the situational awareness of the maritime fleet for subsurface threats and anti-submarine warfare.

Three lines of effort were pursued by the research team, the first two were unclassified dealing with detection of whales and third line of effort was classified processing real field data and is included as a supplemental. The two unclassified efforts affixed commercially available imaging sensors to both manned and unmanned aircraft with the goal of detecting whales at night utilizing bioluminescence. Bioluminescence is emitted light by a chemical reaction from living organism such as fireflies, jellyfish, or marine dinoflagellates [1]. When a pressure differential occurs around the organisms an internal chemical reaction occurs producing emitted light at approximately 475nm [2]. Therefore, the assumption is that it could be possible to detect the emitted light from dinoflagellates to detect movement in the water which may make it possible to detect subsurface targets at night [1].

Many challenges were identified and overcome during the first phase of data collection. The preliminary tests using a low-flying small Unmanned Aerial System (sUAS) with affixed Sony UMC-R10C and 5-band MicaSense RedEdge-MX dual payload showed concerns with the percentages of pixels per image based on the altitude of the aircraft dictating a need to reduce experimental altitude to improve the identification of a marine mammal at shallow depth [1]. Imagery obtained using a Complementary Metal-Oxide Semiconductor (CMOS) based sensor deployed on a general aviation aircraft showed challenges with both the exposure time creating elongated imagery and the need

to filter environmental light to focus the sensor on the specific wavelength needed to detect bioluminescence [1].

Sensor integration issues such as sUAS light pollution were identified as well as default sensor configuration issues preventing the exposure time, shutter speed, and gain needed for successful capture of low intensity blue light at night. The laboratory experiments allowed the team to uncover the most optimal conditions for the sUAS systems and sensors to capture quality data at night by adjusting both firmware sensor setting and mission management software settings to collaborate effectively.

The use of the MicaSense RedEdge-P on the DJI Matrice 300 RTK was the most optimal flight system and sensor system pair used during this research. The sUAS platform is capable of extended flight time compared to other rotary sUAS systems and when combined with the MicaSense RedEdge-P produce some of the best low light images to date for a commercial-off-the-shelf (COTS) system. The DJI Matrice also has a forward-facing built-in camera which allows for the pilot to get live visual sUAS bearing during flight even while flying the MicaSense sensor which does not provide live visual feed back to the controller. This was extremely helpful during sUAS hand catch recovery off the stern of a research vessel at night.

This research project took almost two full years of work to get to the point where the research team, flight system, and sensor systems were mature enough to be able to capture subsurface imagery at night. From the beginning this goal was hard to achieve but the work done by the research team moved the idea several steps forward. Hood Technology is private research group out of Hood River, Oregon, and has partnered with this research team during some of the experiments. They are currently developing an integrated sensor system for the Fire Scout sUAS system with a built-in bioluminescence sensor called PAISO. Working with their team on a custom-built system and using the lessons learned from this research on the capabilities of COTS flight systems and sensors will give the next phase of research a major advantage.

References

[1] J. Goff, A. Elbrecht, and O. Yakimenko, "Challenges in developing nighttime airborne marine mammal avoidance capability," in *OCEANS 2022, Hampton Roads*, Oct. 2022 [Online]. Available: https://ieeexplore.ieee.org/document/9977068

[2] M. Valiadi and D. Iglesias-Rodriguez, "Understanding bioluminescence in dinoflagellates—How far have we come?," *Microorganisms, v*ol. 1, no. 1, pp. 3–25, Sep. 2013.

THIS PAGE INTENTIONALLY LEFT BLANK

ACKNOWLEDGMENTS

I first and most importantly want to thank my wife, Cassie, for her unwavering support and steadfast conviction that I would succeed and do well in this program. Without your support and willingness to listen to my stress-induced venting with a compassion and firm love I would not have gotten this far. I am truly thankful to God for giving me such a wonderful partner on this journey.

I would like to thank Rear Admiral Thomas Q. Donaldson V, USN (ret) for championing this project and his constant support to see this research pushed one step closer to operational impact. I would also like to thank Commander Rob Brodie, USN (ret) who pushed hard to get this research picked up by the Naval Postgraduate School.

During the footage capture portion of the project, Monterey Bay Whale Watch and Jason Berring provided extensive support and training on marine mammal videography and were invaluable in our research.

I am grateful for the partnerships of the local National Oceanic and Atmospheric Administration Unmanned Aerial Systems team led by Lieutenant Commander J. C. Clark and the team at the U.S. Coast Guard station Monterey led by Commanding Officer Lieutenant Matthew Pereya.

Finally, I would like to thank Professor Oleg Yakimenko who chose a budding engineer with absolutely no drone experience and allowed me the opportunity to grow and learn, expanding my horizons here at NPS. Thank you for your wisdom and guidance throughout this project.

THIS PAGE INTENTIONALLY LEFT BLANK

I. INTRODUCTION

As the United States Navy (USN) progresses deeper into the 21st century, the organization's vision is shifting toward a focus on the application and use of unmanned systems. These unmanned assets provide value to the USN mission set through a coordinated range of operational diversity. The Distributed Maritime Operations (DMO) concept outlines the need for integration of these non-traditional assets into the USN strategic decision processes for subsurface object detection, avoidance, and tracking.

The International Maritime Organization (IMO) reports the number of naval and merchant vessels traversing the world's oceans has increased over 320% since 1980 with a linear increase since 2013 of approximately 63,000 newly registered vessels per year and is displayed graphically in Figure 1 [1].

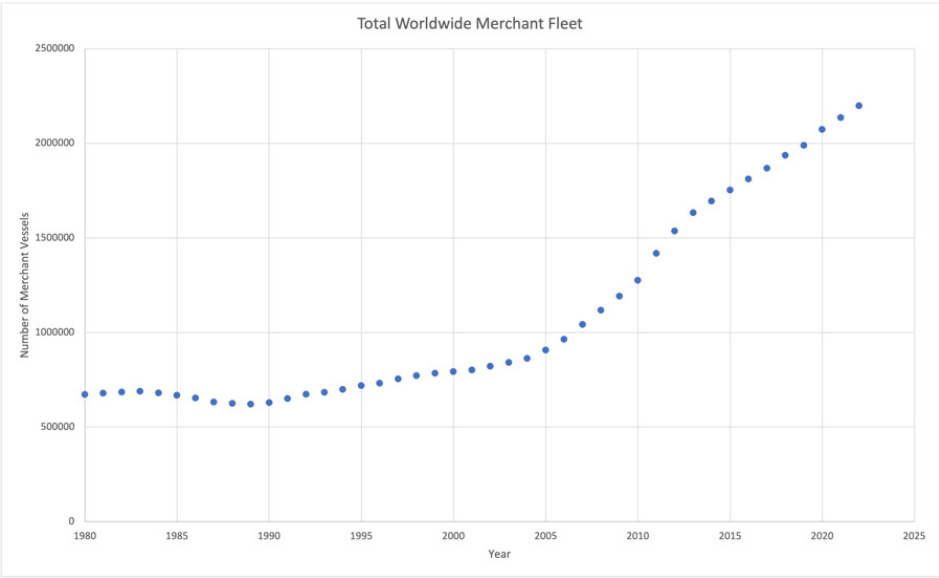

Figure 1. Growth of worldwide naval and merchant vessel fleet reported by the IMO since 1980. Adapted from [1].

The environmental impact of the industrialization of our world's ocean ecosystem is only now starting to be seen. Naval and merchant ships traverse many of the same routes as marine mammals during their annual migrations [2]. Whales are often casualties of the

maritime industry as seen in Figure 2, where a humpback whale was struck by a merchant vessel.

Figure 2. Humpback whales struck by a merchant vessel can be carried far from the impact site. Source: [3].

The USN alongside the United State Coast Guard (USCG) and Merchant Marines need to consider the environmental impact and public perception of the ecological cost of their fleets. With the USN and USCG seeking to modernize and replace depreciating assets, the integration of unmanned systems to expand the vessels lookout range for friendly, enemy, and environmental contacts should be considered.

The threat of subsurface adversaries including criminal organization and foreign militaries is also on the rise as tensions with foreign nations increase [4]. One of the USCG statutory missions is law enforcement within our national waters as well as internationally under treaties with the United Nations. Figure 3 shows the USCG overtaking a criminal semi-submersible in the Eastern Pacific Ocean.

Figure 3. USCG Cutter Munro (WMSL-755) crew members inspect a self-propelled semi-submersible on June 19, 2019, in international waters of the Eastern Pacific Ocean. Source: [5].

This research effort desires to assess the feasibility of using commercially available unmanned aircraft alongside standard imaging sensors to increase the situational awareness of the maritime fleet. This thesis has two parts—unclassified (dealing with detection of whales) and classified (dealing with real field data) which is included as a supplemental. The unclassified portion of the thesis is organized as follows. Chapter II represents a conference paper submitted to the IEEE Oceans 2022 conference held in Hampton Roads, VA. Chapter III contains further analysis of the data collected during the experiments included in Chapter II as well as new data from additional experimentation; Chapter IV summarizes all findings and provides recommendations for future work.

The classified portion of this work is included as the second supplemental to this report alongside two additional supplements that support the analysis conducted in the classified report.

THIS PAGE INTENTIONALLY LEFT BLANK

II. MANUSCRIPT SUBMISSION

A. CHALLENGES IN DEVELOPING NIGHTTIME AIRBORNE MARINE MAMMAL AVOIDANCE CAPABILITY

A version of this chapter was submitted in October 2022 to the Oceans 2022, Hampton Roads Conference and published by IEEE as: J. Goff, A. Elbrecht, and O. Yakimenko, "Challenges in Developing Nighttime Airborne Marine Mammal Avoidance Capability," in *OCEANS 2022, Hampton Roads*, Oct. 2022 [Online]. Available: https://doi.org/10.1109/OCEANS47191.2022.9977068.

This publication is a work of the U.S. Government as defined in Title 17, United States Code, Section 101. Copyright protection is not available for this work in the United States. IEEE will claim and protect its copyright in international jurisdictions where permission from IEEE must be obtained for all other uses, in any current or future media, including reprinting/republishing this material for advertising or promotional purposes, creating new collective works, for resale or redistribution to servers or lists, or reuse of any copyrighted component of this work in other works.

B. INTRODUCTION

Marine mammal collision by naval and merchant vessels is a growing safety and environmental concern [3]. In 2007, the International Whaling Commission (IWC) launched a long-term initiative to collect and analyze information about reported marine mammal ship strikes, both historic and current, aiming at identifying "hot spots" where large numbers of whales coincide with busy shipping lanes [6].

As part of the IWC initiative, researchers from Austral University of Chile placed satellite trackers on 15 whales off the coast of northern Chilean Patagonia in 2019 and overlaid it with publicly available shipping information showing that whales feed in spaces subject to intense marine traffic [7]. Figure 4 shows a heat map created from vessel traffic and whale migration data indicating that the Ancud Gulf is a high activity area for both.

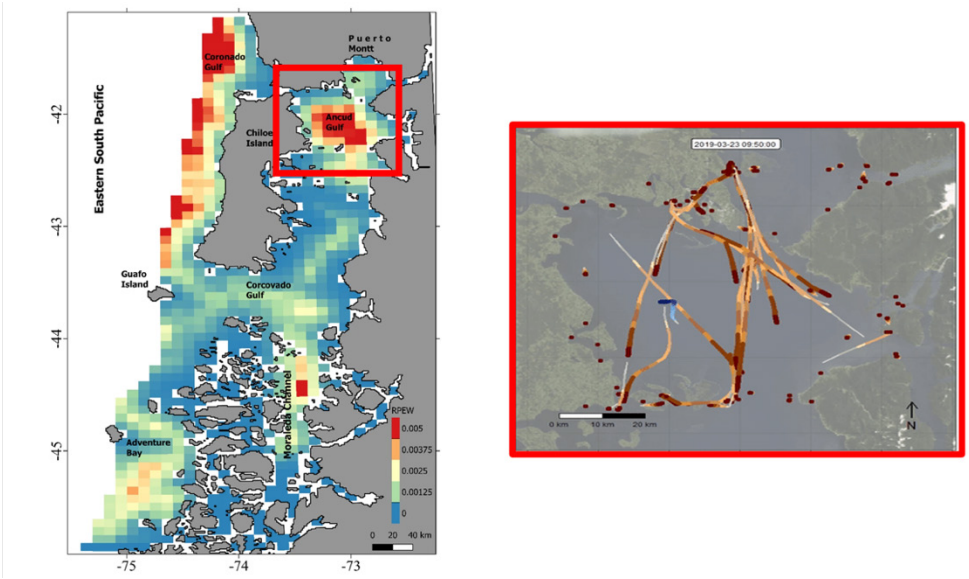

Figure 4. Tracker data from merchant vessels and whales in northern Chilean Patagonia. Adapted from [7].

The researchers made a real time visualization of one of the whales' tracker data and the merchant vessels automatic identification system (AIS) data to show that a whale in the Ancud Gulf will contend with around 1,000 merchant vessels as indicated by the blue dot with a tail on the enlarged visual in Figure 4. To date, the IWC has identified 12 hot spots and has logged at least 1,200 collisions between ships and whales globally. Indeed, for every accident observed and reported there will be many others completely unnoticed. Quite often, the injured whales are found dead because of the injury that was likely a result of blunt force trauma to the chest. Since whales have no natural predator the most probable reason is the whale collided with one of an increasing number of maritime vessels.

C. BACKGROUND AND LITERATURE REVIEW

This section presents background information on small Unmanned Aerial Systems (sUAS), the nature of bioluminescence, and a discussion of commercial-off-the-shelf (COTS) available sensors applicable for low-light detection of moving objects in shallow water.

1. Small Unmanned Aerial Systems

Rapid advancement in sUAS and image processing technology have led to their extensive deployment and operational integration. Currently technology, such as radar, is insufficient in marine mammal detection and there is no other system in place for nighttime marine mammal detection in real time. The use of sUAS leveraging bioluminescence for this application has been proposed after operational photography of a school of tuna was captured off the coast of California shown in Figure 5.

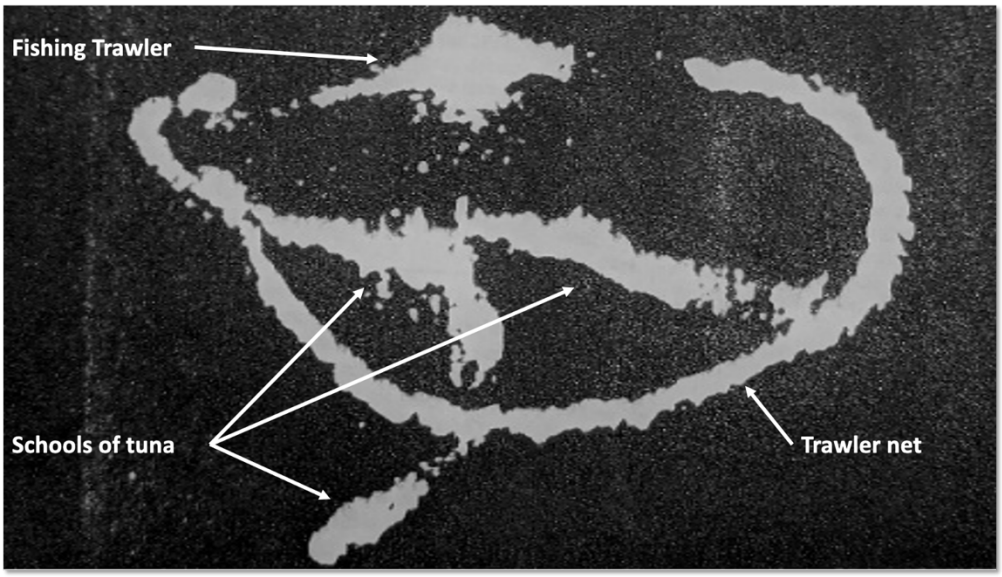

Figure 5. A 1974 image of fish escaping from a trawler's net off the California coast. Source: [8].

The use of aerial imagery for detecting subsurface marine mammals is not new and has been tested successfully many times in daylight operations [9]. This experiment seeks to determine the field feasibility of combining this naturally occurring image enhancement phenomena with advanced image processing to further research in nighttime marine mammal avoidance. As an example, Figure 6 shows the processing of daylight imagery of a humpback whale in Monterey Bay, California.

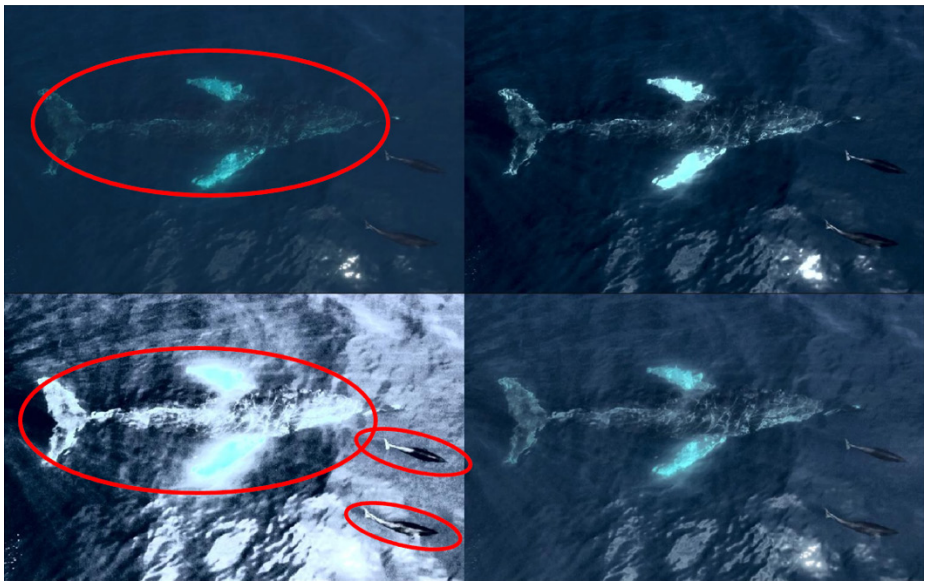

Figure 6. Visual enhancement of captured electro-optical imagery of a humpback whale in Monterey Bay, CA. Source: [10].

The image was captured using a high-definition red, green, blue (RGB) camera mounted on a rotary sUAS system. The image in the top left is the original and the other three use varying image enhancement methods. The bottom left photo uses contrast enhancement and shows three separate marine mammals, one humpback whale and two dolphins, more easily identified than in the original.

2. Bioluminescence

This section convers the nature of bioluminescence and discusses the application of sensor technology to detected emitted bioluminescent light.

a. Nature of bioluminescence

Bioluminescence is emitted light by a chemical reaction from a living organism. Fireflies and some jellyfish are well-known examples for bioluminescence. A special group of marine organisms are dinoflagellates. Many species emit light via bioluminescence especially when they are agitated by pressure forces associated with moving objects [11].

The emitted light is blueish and has a wavelength of approximately 475nm [11]. Therefore, the assumption is that it could be possible to detect the emitted light form the

dinoflagellates to detect movement in the water which may make it possible to detect whales at night. Monterey Bay, California, and the surrounding area is a concentrated region for both dinoflagellates and comb jellies which concentrate during different seasons of the year leading to almost year-round bioluminescent activity in the region. As an example, Figure 7 depicts bioluminescent waves off the coast of Big Sur near the Bixby Bridge just south of Monterey, California [12].

Figure 7. Dinoflagellates illuminate shorelines waves off the coast of Big Sur near Monterey Bay, California. Source: [12].

b. Sensor detection of bioluminescent light

Bioluminescent light emitted by marine organisms has the potential to be utilized to highlight the shallow water and subsurface movements of any object or wildlife that creates a pressure differential high enough to agitate the marine organisms causing light emission. Sensor systems to detect low levels of 475nm light at night must be developed or repurposed to make use of this naturally occurring object enhancement phenomenon.

Other obstacles also exist that make the utilization of bioluminescence a challenge. First, lunar light or surface reflections can overwhelm the luminescent intensity of the bioluminescent light where it cannot be easily detected, thus highest probability of

detection will most likely occur during new moon periods or after moon set when the moon has fallen below the horizon during night hours.

Another challenge is predicting the movement and concentrations of marine organisms which produce bioluminescent light to make sure that the luminescent intensity of the light produced is high enough to register with current commercial sensors.

Lastly, combining the events of marine mammal movement in bioluminescent blooms during the proper lighting conditions to detect movement with commercial sensors is difficult to achieve. The focus of this initial research is to look at commercial sensor technology for easy repurposing to detect bioluminescent light and to conduct controlled experimentation to understand the feasibility of this thesis.

3. Current State Of COTS Light-Weight Sensor Technology

To detect the emitted light from dinoflagellates this research intends to use two different approaches. The first approach relies on using a small sensor that can be carried aboard a sUAS. In this case, the major constraint is the size of the sensor. The search for all feasible sensors resulted in choosing the 10-band MicaSense Blue/RedEdge-MX dual camera system and combined Sony UMC-R10C and 5-band MicaSense RedEdge-MX shown in Figure 8 [13].

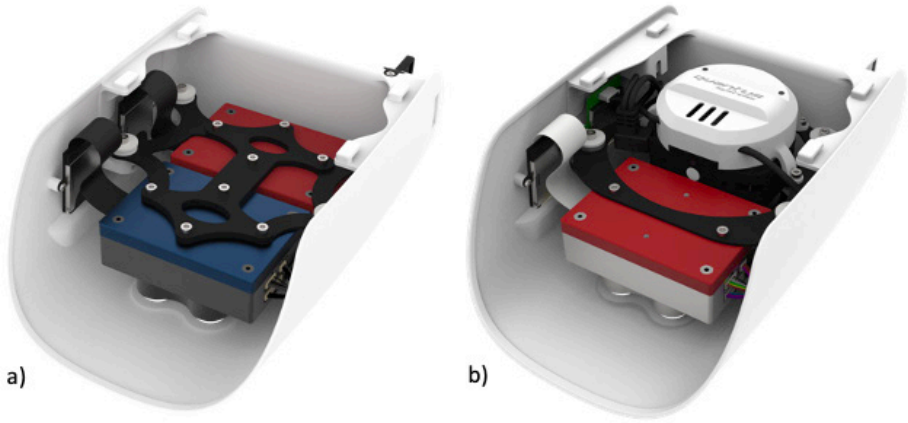

Figure 8. MicaSense 10-band dual camera system (a), and combined Sony UMC-R10C and 5-band MicaSense RedEdge-MX (b). Source: [13].

The dual sensor shown in Figure 8(a) has a weight of 550g and allows for synchronized capture of 10 separate wavelength bands ranging from 444nm to 842nm at 1.2 megapixels (MP) per band. Figure 8(b) shows the Sony UMC-R10C 20MP RGB sensor with 20mm lens and 5-band MicaSense RedEdge-MX with a combined weight of 537g. The MicaSense RedEdge-MX has five sperate cameras with a global shutter, which are centered on five different wavelength regions: Blue (475nm center, 32nm bandwidth), green (560nm center, 27nm bandwidth), red (668nm center, 16nm bandwidth), red edge (717nm center, 12nm bandwidth), and near-infrared (842nm center, 57nm bandwidth) [14]. The length of exposure (the amount of time the global shutter is "open" and recording light) ranges from 0.066ms to 24.5ms [15].

Another approach is to find the most sensitive (still affordable) sensor, not constrained by the size and weight assuming it will be carried using an appropriately equipped general aviation aircraft. Figure 9 shows the SBIG STC-428-OEM from Diffraction Limited with a Complementary Metal-Oxide Semiconductor (CMOS) sensor, high light sensitivity, and a fast readout [16].

Figure 9. SBIG STC-428-OEM scientific CMOS imaging camera. Source: [16].

The CMOS sensor was modified for use on a manned aircraft by combining it with a Nikon lens with high shutter speed and a bandpass filter for blue light detection of

bioluminescence [17], [18]. With these modifications the detection of light emitted by bioluminescence caused by the movement of whales at night should be possible. The whole assembly weights 1,115g and is housed within a three-dimensional (3-D) printed enclosure as shown in Figure 10.

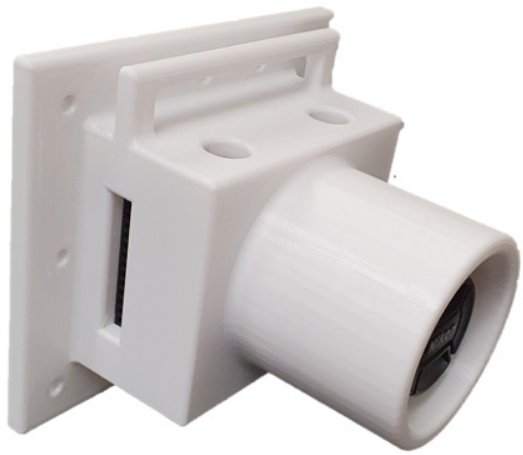

Figure 10. CMOS imaging camera assembly mounted within a custom 3-D enclosure. Source: [10].

D. DATA COLLECTION AND PROCESSING

This section describes the field experiments that were conducted to collect low light multispectral imagery and the multistep procedure that was developed and applied to post process the data.

1. Test Setup

Both sensors described in Chapter II, Section C.3 were integrated with sUAS and manned aerial platforms as follows.

a. sUAS integration

The Quantum Trinity F90+ electric vertical take-off and landing (eVTOL) sUAS has sensors integrated in its belly and is shown in Figure 11.

Figure 11. Quantum Systems Trinity F90+ eVTOL sUAS equipped with multispectral sensor. Source: [10].

This sUAS features eVTOL capability combined with the forward thrust energy efficiency of a fixed wing sUAS for a maximum flight time of 90 minutes per battery [19]. The sUAS is launched near the shoreline and then flies off and executes a preprogrammed search pattern over the ocean near La Selva Beach, California, where whales are usually spotted. The maximum altitude for this experiment is 120m (400ft) above the mean sea level (MSL) and the cruise speed is 17m/s (33kts). For the MicaSense RedEdge-MX at this altitude each image captures approximately 102m×77m area and is tied to each separate band with the resolution of 1,280×960 pixels [15]. The Sony UMC-R10C 20MP RGB has an aspect ratio of 3:2 with a resolution of 5,456×3,632 pixels [20]. Imagery overlap is programmable in the mission management software and can be adjusted based on mission requirements. Image capture timing is automatically adjusted based on this overlap setting and the current environmental conditions such as wind.

b. Manned aircraft integration

The modified SBIG STC-428-OEM CMOS sensor was mounted within the custom 3-D enclosure on the right-wing strut of a general aviation aircraft using a Federal Aviation Administration (FAA) approved mount in the face down position as shown in Figure 12.

Figure 12. General aviation aircraft with affixed image capturing platform equipped with the low-light SBIG CMOS-based sensor. Source: [10].

This sensor has about the same aspect ratio as the Sony UMC-R10C sensor with a 1.7 times lower resolution of 3,208×2,200 pixels [20]. The camera operator resides at the back seat taking still imagery and adjusting exposure settings as needed. Compared to the sUAS in Figure 11, the manned aircraft flies at an altitude of 610m (2,000ft) MSL at 46m/s (90kts). At this altitude each image captures and area of approximately 174m×20m. If images are taken 3.78s apart, there is no overlap with the previous image.

2. Data Processing Setup

All data for these experiments were post-processed after completion of the experimental data collection. No real time processing was done, though this is an area for further development once the sensor challenges have been overcome.

Data for the experiments were captured from the sensors onto secure digital (SD) memory cards. The SD cards were formatted according to the sensor manufacturing specifications, and normally formatted directly from the sensor or sensor software. After completion of any experimental run the SD cards were removed and the data was transferred to a computer for processing. The experimental data was backed up from the computer to an external file hosting service for long term data storage.

A combination of Agisoft and MATLAB software suites were used to post-process the imagery. Agisoft photogrammetric processing allows for creation of orthomosaic overlays of sensor data by stitching together images from preprogrammed mapping patterns into a single orthographic image. MATLAB Image Processing Toolbox allows for detailed analysis of the imagery specifically enhancement to bring out underlying or fine detail such as that seen in Figure 6.

E. PRELIMINARY ASSESSMENT OF SENSOR DATA

This section provides a preliminary analysis of the feasibility of finding whales using the two available sensors as described in Chapter II, Section C.3. This analysis is based on a few samples of data collected to date.

1. Multispectral Sensor Imagery

Figure 13 illustrates a physical resolution of the imagery taken using the MicaSense RedEdge-MX sensor when flown at different altitudes above MSL.

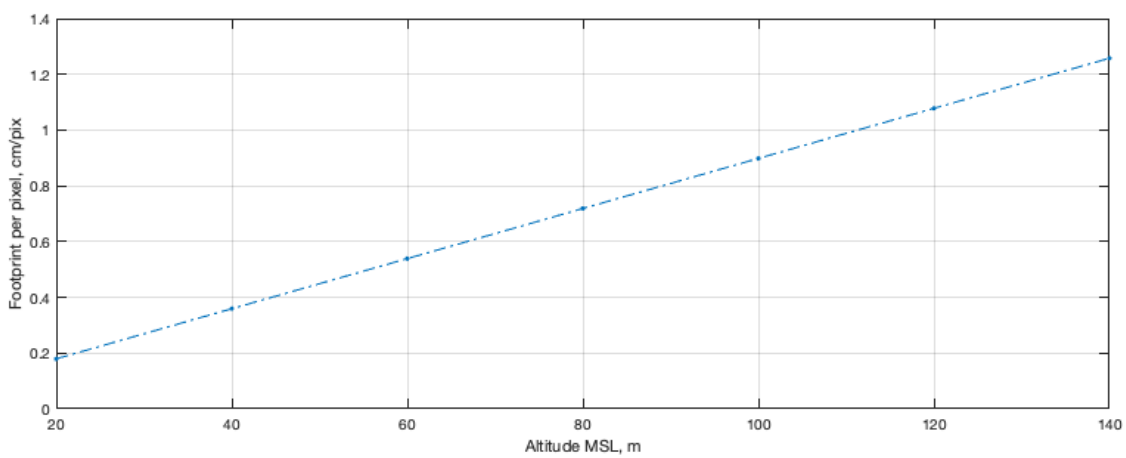

Figure 13. Footprint per pixel for MicaSense RedEdge-MX sensor flown on a sUAS. Source: [10].

Simple calculations show that the resolution of this sensor if flown at 120m (400ft) MSL would have a gray whale of a typical length of about 14m and width of 3.5m to

occupy 7,666 pixels or 1% of the image. The assumption is that in the presence of bioluminescence, it should suffice to detect or even identify a whale.

The strength of bioluminescence emission would then define sensor exposure. At night, it may require extended time to capture enough emitted light. That is where a problem arises. With a sUAS flying at low altitude and a cruise speed of 17m/s (33kts), compatible with the speed of the ship, longer exposure which would be required to capture weak bioluminescence emission, means image shift. To this end, Figure 14 shows this shift in pixels for different altitudes and exposure time. As seen, for longer exposure time this shift can be relatively large, especially for the lower altitudes.

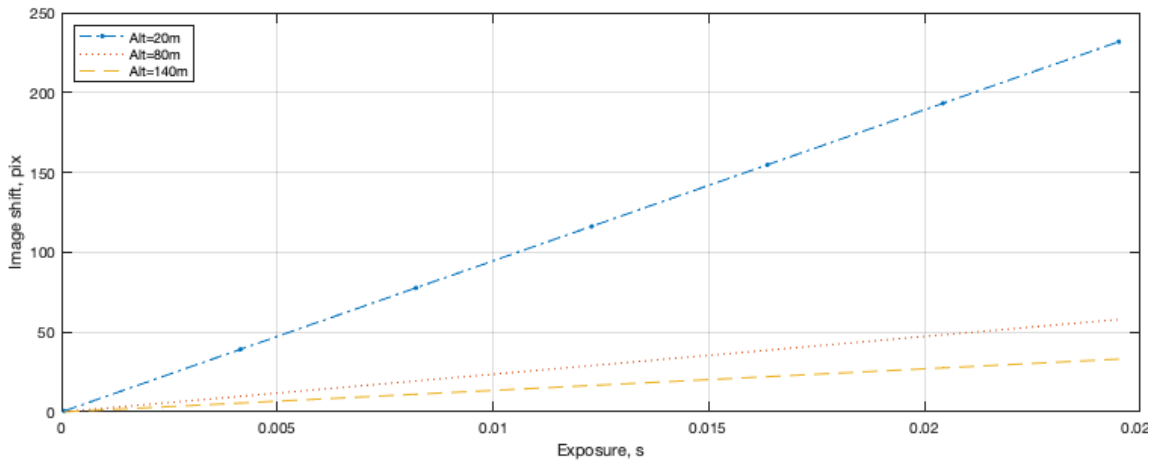

Figure 14. Image shift for a low-flying fixed wing sUAS cruising at 17m/s. Source: [10].

Figure 15 presents a sample of imagery of a submerged humpback whale captured in Monterey Bay, California with the MicaSense RedEdge-MX sensor from approximately 30m (100ft) MSL during daylight.

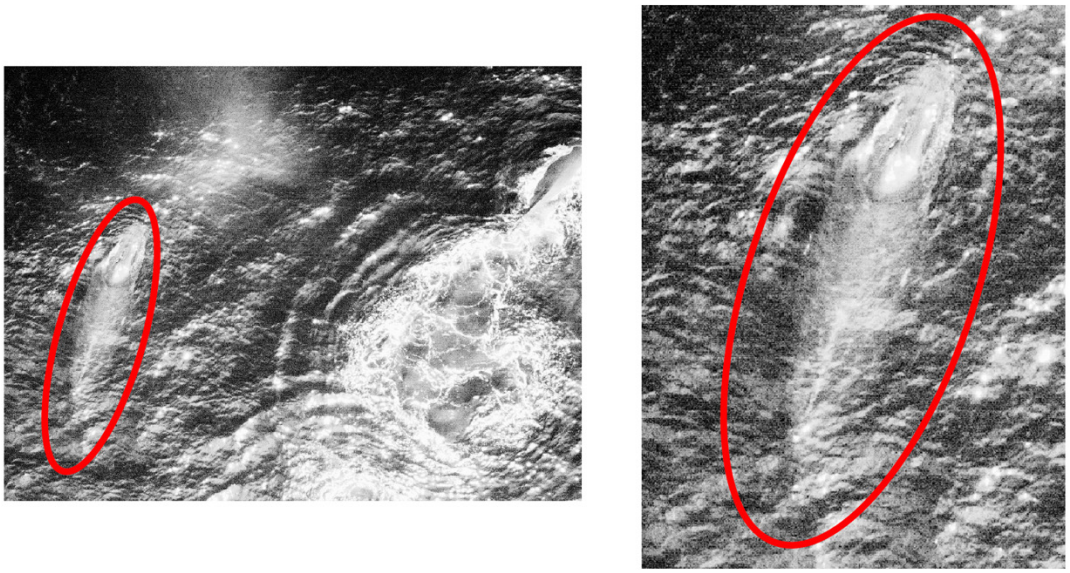

Figure 15. The Blue-band grayscale image of a humpback whale in Monterey Bay captured with MicaSense RedEdge-MX from a low-flying sUAS with enhanced contrast using histogram equalization. Source: [10].

Specifically, this figure shows the full-size blue band image on the left and an enlarged portion with a humpback whale on the right. While other spectrum band images appear to be about the same, if assessed with a naked eye, when conducting image processing to detect a whale all five bands complement each other making a detection algorithm more reliable and precise.

2. CMOS Sensor Imagery

Like the analysis presented in Chapter II, Section E.1, Figure 16 shows a footprint in cm/pix of a CMOS sensor flown on a general aviation aircraft when flying at different altitudes.

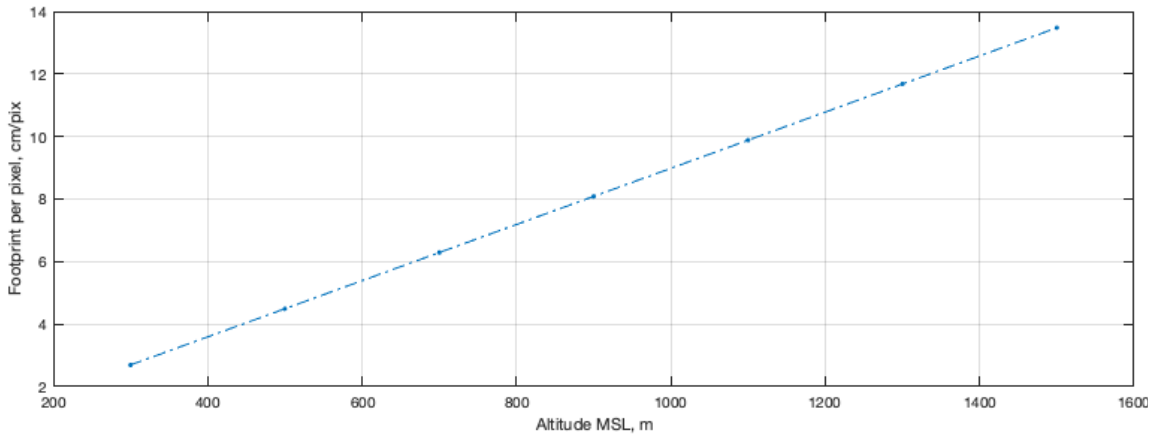

Figure 16. Footprint per pixel for low-light sensor flown on a general aviation aircraft. Source: [10].

Using this data, a 14m×3.5m whale would occupy 19.3% of the low-light sensor when flown at 400m MSL and 5.5% at 1,400m MSL. While this performance of the black and white low-light sensor is still acceptable, the image shift for a much faster flying aircraft (46m/s or 90kts) becomes a real issue as shown in Figure 17.

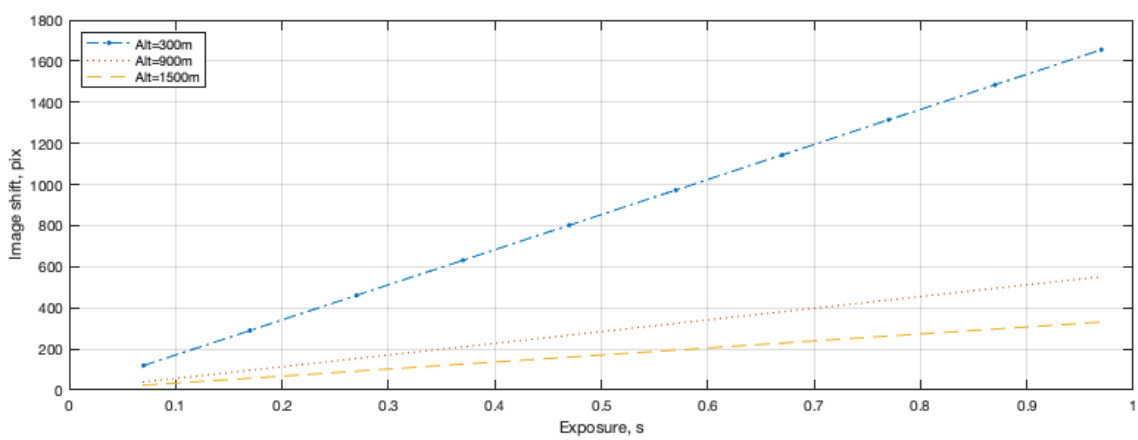

Figure 17. Image shift for CMOS sensor mounted on a general aviation aircraft flying at a typical cruise speed. Source: [10].

To illustrate this shift, Figure 18 shows an example of imagery taken with just 0.07s exposure when flying at 1,200m (4,000ft) MSL at 40m/s (77kts).

Figure 18. Image with a 0.07s exposure when flying at 1,200m (4,000ft) MSL at 40m/s (77kts). Source: [10].

Specifically, Figure 18 shows a night image of a bridge superimposed over the daytime image featuring fuzzy streetlights. This image shift lies at the very left end of the lower curve of Figure 17. Figure 19 shows the Monterey Bay, California Fisherman's Wharf in daylight, (a), and the nighttime illumination of the same object, (b).

a) 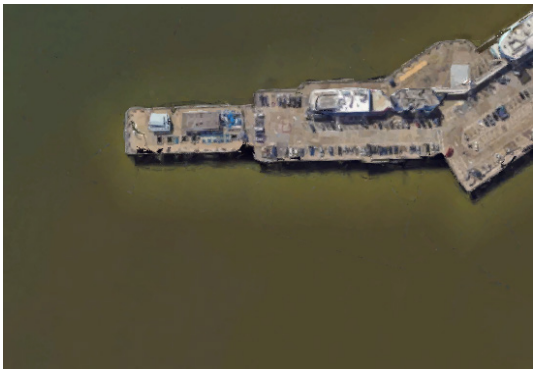 b) 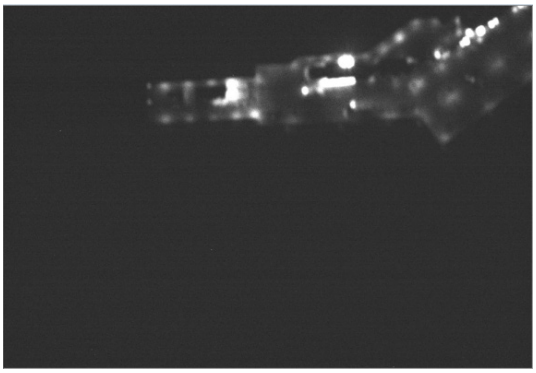

Figure 19. Monterey Bay, California Fisherman's Wharf in daylight, (a), and the nighttime illumination of the same object, (b), with 0.7s exposure at 1,200m MSL and speed of 40m/s. Source: [10].

Obviously, with a much longer exposure, a whale would appear not as it would be seen during the daytime. Figure 20 intends to convey the effect of the camera exposure

time for a 14m×3.5m whale flying at 1km MSL at a cruise speed of 46m/s with a footprint of 288m×198m.

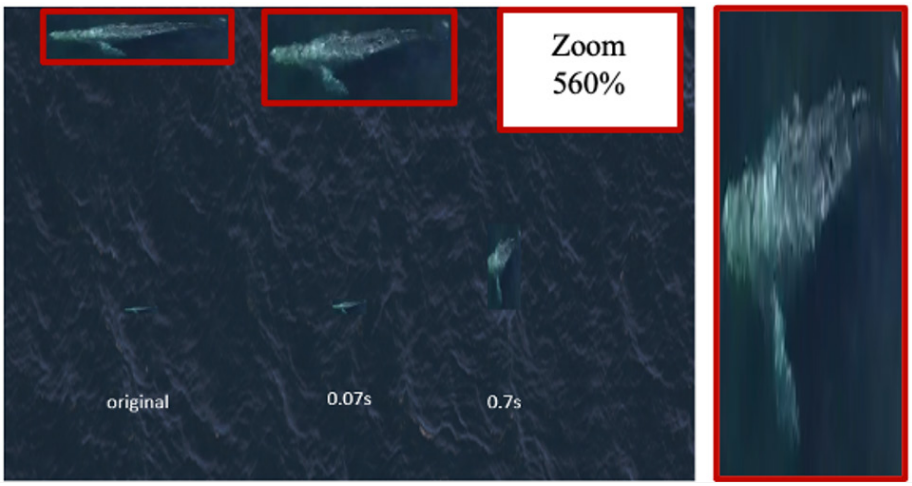

Figure 20. Artistic representation of the effect of elongated exposure time (true to scale). Source: [10].

The effect of the stretched image, caused from the movement combined with the exposure time, could be calculated and processed to get a clear image. It would also be possible to add a stack of images with a lower exposure time together. But if the observed object changes its pose or shape, as maybe the case if a whale moves, the result will not be a sharp image in both cases.

To ease the process of finding a whale in the ocean at night using the light from bioluminescence it is necessary to avoid other light emitting sources and reflections. Therefore, a narrow blue bandpass filter with a fitting bandwidth of 460nm to 490nm was used and the effect is visualized in Figure 21 [17], [18].

a) b)

Figure 21. The 70s exposure images taken with (a) and without (b) bioluminescence filter. Source: [10].

To illustrate the effect of applying this filter using a simple example consider the images shown in Figure 21, they both show the same shoreline lightly illuminated by the moon as seen by the CMOS-based sensor mounted on a tripod with an attitude somewhat like that of Figure 10. What is seen in the field of view is a water edge, bush alga (towards the upper portion of the image), and an illuminated sand path. With an exposure time of 70s the sensor can create a good visible black and white image of a non-dynamic environment. The first observation is that since there was no bioluminescence present at the time these two 70s exposure images were taken, Figure 21a, depicting the case of an applied filter with all outlying wavelength blocked, looks very dark. The second observation is that when the blue filter is removed as shown in Figure 21b, night environment shows up very clear compared to Figure 21a.

Indeed, the two challenges of applying a narrow blue bandpass filter and using long exposure time settings make getting a clear image of a moving whale quite difficult, especially in the case of weak bioluminescence emission. Future experimentation will be aimed at the ways to mitigate the effects of these two challenges, which includes developing the corresponding image processing and enhancement algorithms.

F. CONCLUSION AND RECOMMENDATIONS

1. Conclusion

This paper presented the initial assessment of an idea of nighttime airborne marine mammal avoidance capability. The preliminary tests using a low-flying sUAS with affixed Sony UMC-R10C and 5-band MicaSense RedEdge-MX dual payload showed concerns with the percentages of pixels per image. These concerns were based on the altitude of the aircraft dictating a need to reduce experimental altitude based on the sensor specifications to improve the identification of a marine mammal at shallow depth. Imagery obtained using an affixed SBIG STC-428 Photometric CMOS-based sensor deployed on a general aviation aircraft showed challenges with the exposure time creating elongated imagery and the necessary need for filter usage to focus the sensor on the specific wavelength of light needed for the detection of bioluminescence.

2. Recommendations for Future Work

Moving forward the authors will be focused on three primary areas for data collection. First, reducing the altitude of the sUAS during flight and conducting nighttime experimentation with Sony UMCR10C and 5-band MicaSense RedEdge-MX dual payload. Second, improving the quality of SBIG CMOS-based sensor imagery using a shutter to reduce elongation of images due to exposure time. Lastly, developing advanced image processing algorithms which can isolate minute changes in image intensity from the sensor systems to detect low levels of bioluminescent light at night.

III. ADDITIONAL EXPERIMENTATION AND ANALYSIS

Multiple field experiments were conducted by the NPS team during this research project, with two large scale joint experiments focused on sUAS data collection. The first joint experiment was executed in the fall of 2022 and was a collaboration between eight different federal, state, and local agencies whereas the second was a follow-on experiment done in the winter of 2023 with four of the original agencies. This section covers the planning, execution, and data evaluation of both joint experiments as well as laboratory testing of the sUAS sensor system between data collections.

A. JOINT EXPERIMENT 1: SUAS LAUNCHED FROM SHORELINE

The first experiment was conducted on the evening of September 27, 2022, as a joint effort between NPS, the USCG, Monterey Bay Aquarium Research Institute (MBARI), Insight Up Solutions, the National Oceanic and Atmospheric Administration (NOAA), the Naval Research Lab, Monterey Bay Whale Watch, and Upwell. A visualization of each of the member agencies logos can be seen in Figure 22.

Figure 22. Visualization of the member agency logos who partnered during the September 27, 2022, experimentation. Adapted from [21]–[28].

1. Planning Phase

The initial planning of this experiment started in the summer of 2022 as a collaboration between NPS, NOAA, and MBARI to share sUAS resources. MBARI

contributed data from their Dorado class autonomous underwater vehicle (AUV) shown in Figure 23.

Figure 23. MBARI Dorado class AUV used in Joint Experiment 1. Source: [29].

This AUV system has a suite of onboard ocean chemistry sensors that can detect the concentration of chlorophyll and sea temperature to give researchers an understanding of bioluminescent potential for the area. Figure 24 shows average bioluminescent potential in photons per liter (ph L^{-1}) based on latitude and time of year in Monterey Bay.

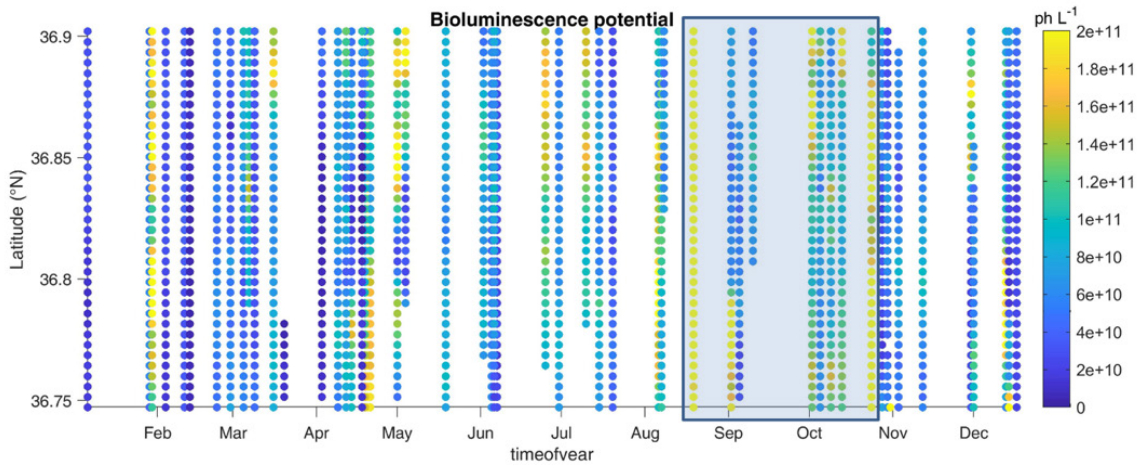

Figure 24. Average bioluminescent potential for Monterey Bay, CA based on latitude and time of year. Adapted from [30].

From Figure 24 it is apparent that some of the most consistent bioluminescent activity occurs from mid-September through October as well as in mid-February through mid-March. Based on this information provided by MBARI the research team planned the initial data collection experiment for mid to late September based around the new moon phase to limit external light pollution and better see bioluminescent light. The new moon window for September 2022 occurred roughly from the 25th through the 27th giving a three-day window of operations pending weather and flight conditions [31].

The launch location was from the Monterey Bay Academy (MBA) airfield which NPS has a valid FAA Certificate of Authorization (COA). Figure 25 depicts a heatmap of the bioluminescence intensity data from Figure 24 overlayed on a chart of Monterey Bay with the identified locations of the MBA launch site, the USCG small boat launch area, and the track line of the MBARI AUV in black.

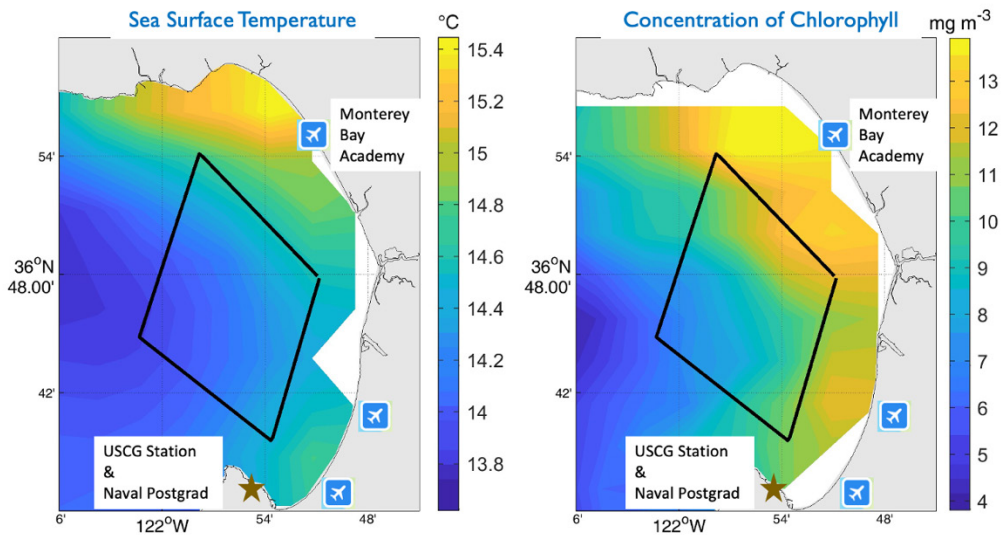

Figure 25. Heatmap of bioluminescent intensity for Monterey Bay with sUAS launch location, USCG small boat pier, and AUV track line. Adapted from [30].

Using the information gathered from MBARI and NOAA, an operational concept was created to depict the experimental goal of the overflights of both the sUAS and general aviation aircraft from Chapter II, Section D, and is shown in Figure 26.

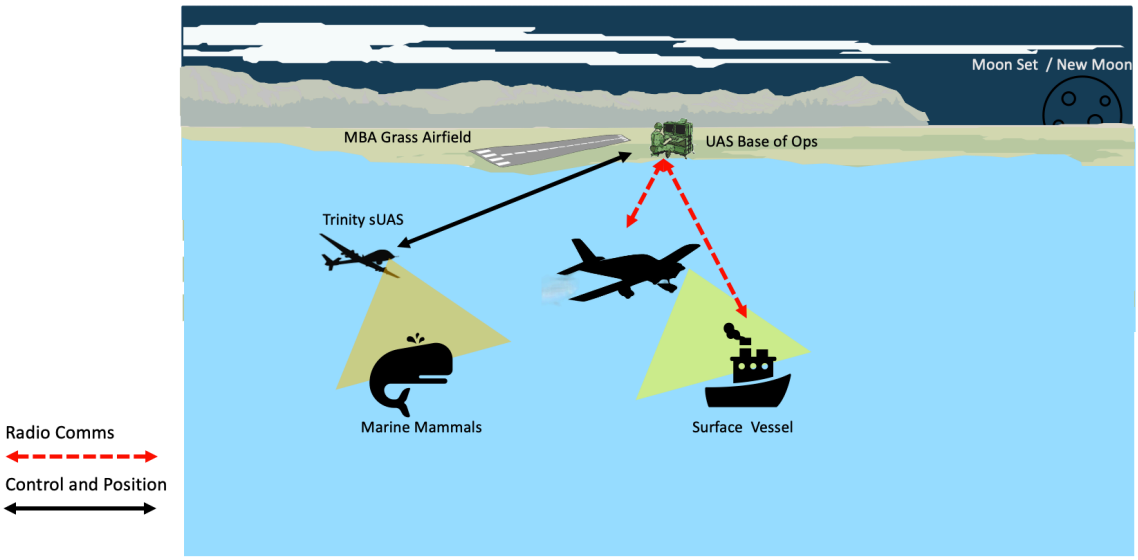

Figure 26. Operational Concept (OV-1) for the September 27, 2022, Joint Experiment 1.

As seen in the OV-1 there were three operational targets identified for the experiment. First, the USCG Station in Monterey, CA volunteered vessel time to transit the area during the experiment window as a surface asset. The vessel used was a 47-foot Motor Lifeboat (MLB) and is depicted in Figure 27.

Figure 27. USCG MLB from Station Monterey, CA. Source: [32].

Second, the MBARI AUV from Figure 23 was stationed within the predefined flight area and programmed to do a circular pattern at approximately 1 to 3 meters depth. Third, was the hope that we would capture any marine mammal during our flight. The first two targets were primary to add an experimental control for the proof of concept.

2. Data Collection

The experiment window ran from September 25 through September 27, 2022, and all data was collected from the sUAS on September 27. The MBARI AUV was prepositioned starting the night of the 25th to gather ocean chemistry data. Due to the cloud ceiling the general aviation aircraft was unable to fly over the target area so all data was collected with the Trinity F90+ eVTOL sUAS from Chapter II, Section D.1.a.

Two flights were conducted on the evening of September 27, 2022. The first flight was flown by the Trinity F90+ sUAS over both the USCG MLB and the MBARI AUV with all flight information visualized in Figure 28.

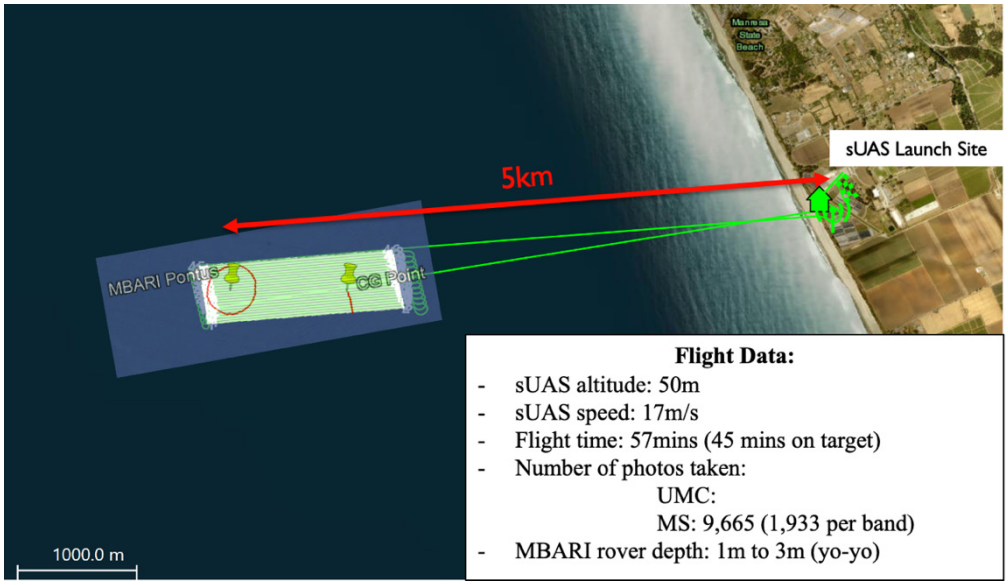

Figure 28. Trinity F90+ flight 1 information.

Figure 28 shows that the initial flight took approximately one hour to fly an east to west grid patter over the flight area and was approximately five kilometers from the launch

site. In aviation terms this is referred to as beyond visual line of sight (BVLOS) and normally is not allowed for sUAS flight. Prior to this flight a risk analysis was conducted by the research team and submitted to the FAA for approval. The FAA gave us the concurrence to proceed under our already issued COA with MBA.

Approximately 9,600 images were captured by the dual imaging payload of the MicaSense RedEdge-MX and Sony UMC shown in Figure 8b. The MicaSense sensor captured images well, but the Sony UMC sensor data was lost due to file corruption. Of the 9,600 images captured approximately 1,900 were captured by the blue band sensor centered on 475nm.

A second flight was conducted over the same area but only over the MBARI AUV target. At the conclusion of the first flight the USCG MLB was called away to conduct a search-and-rescue mission. The flight grid was changed for the sUAS to conduct an east to west grid immediately followed by a north to south grid over the MBARI AUV coordinates. The MBARI AUV continued the same circular station as the first flight but maintained a constant 1m depth and maximum speed of approximately 3kts. The flight data from this flight is visualized in Figure 29.

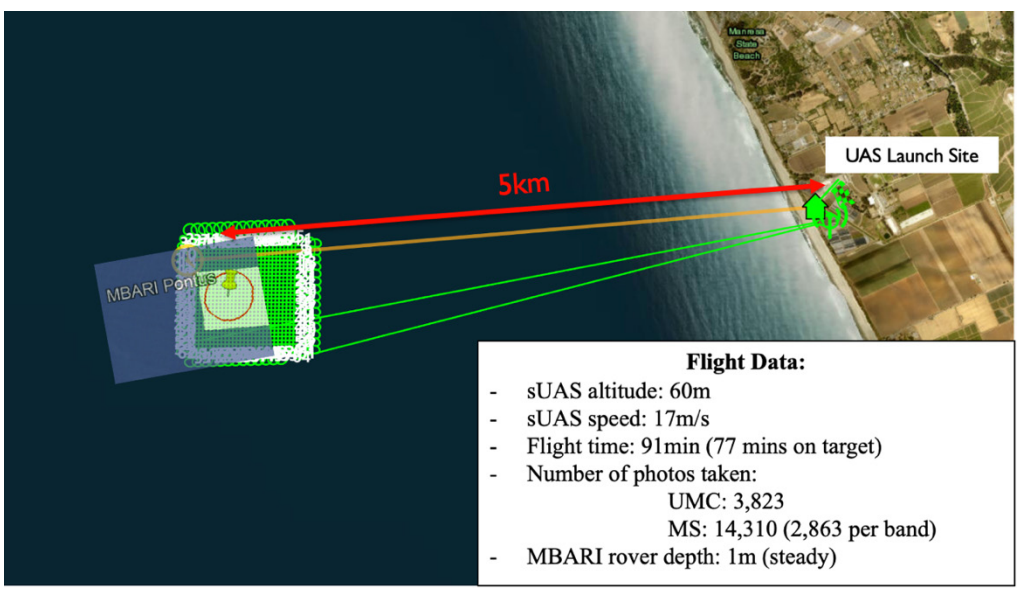

Figure 29. Trinity F90+ flight 2 information.

Figure 29 shows that the second flight took approximately 1.5hrs to fly and occurred approximately five kilometers from the launch site BVLOS. Approximately 18,100 images were captured by dual imaging payload of the MicaSense RedEdge-MX and Sony UMC shown in Figure 8b. The MicaSense imager capture 14,310 images with approximately 2,860 captured by the blue band sensor centered on 475nm.

3. Data Analysis

All data analysis was conducted in MATLAB using the Image Processing Toolbox and all scripts written for MATLAB are included in the Appendix to this thesis. To fully understand the data analysis conducted a few terms need to be defined so that there is consistency throughout the analysis. First, all the MATLAB analysis focused on image intensity and this term is different when referring to both grayscale and RGB images. RGB imagery is the combination of red, green, and blue channels of light with each channel having a specific intensity profile ranging from 0 to 255 that it adds to create the overall color of the image. A grayscale image is only the result of light intensity on a single sensor pixel and at 0 or no intensity, shows as black, and at 255, or high intensity it shows white producing a monochromatic image.

Each sensor is different in how it handles intensity, and the scale is not always consistent from sensor to sensor, therefore normalization of the data is done so that data can be easily compared across sensors. Normalization of intensity data is achieved by dividing a single instance intensity value by the maximum registered intensity or maximum capable intensity. For a normal grayscale sensor, you would divide any single intensity reference value by 255 to get the normalized value on a range of 0 to 1.

Finally, image saturation as discussed in this analysis refers to the depth of color at a specific range including grayscale. The MATLAB Image Processing Toolbox uses a function, “imadjust,” which adjusts the image intensity to saturate the bottom 1% and top 1% of the intensity values increasing image contrast or distinguishability.

a. Mission 1 : Flight data shown in Figure 28

Once the mission was completed all data was transferred from the camera media to an external hard drive for post processing in MATLAB. The images capture from the Sony UMC-R10C were corrupted from this first mission. The images captured from the MicaSense RedEdge-MX were processed first by calculating the maximum, minimum, and average change in intensity for the 1,933 blue band images. This was done using the script in the Appendix, Section A, and the graphic is shown in Figure 30.

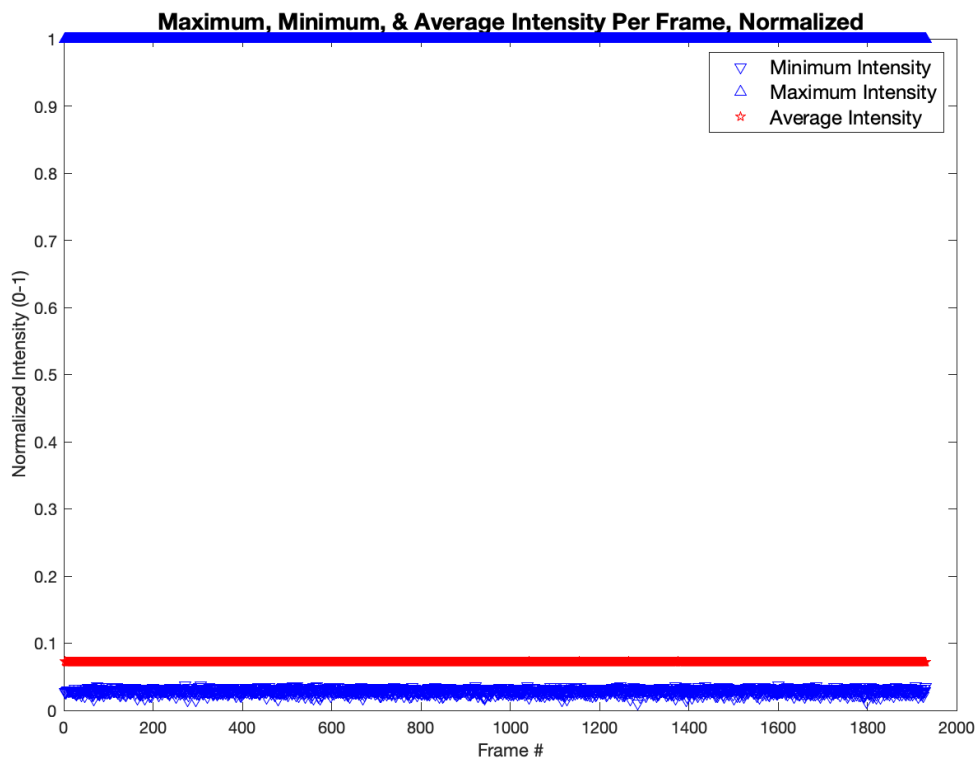

Figure 30. Maximum, minimum, and average change in intensity, normalized, for the blue band centered on 475nm from the MicaSense RedEdge-MX for Mission 1.

The information shown in Figure 30 is interesting in that it shows no change in intensity across the 1,933 blue band images which is extremely improbable and hints at an issue with the image data, experimental procedure, or equipment. A second analysis was

conducted on the entire range of photos for all 5 bands using the MATLAB script in the Appendix, Section B, where intensity was plotted on a normalized scale from 0 to 1 and is shown graphically in Figure 31.

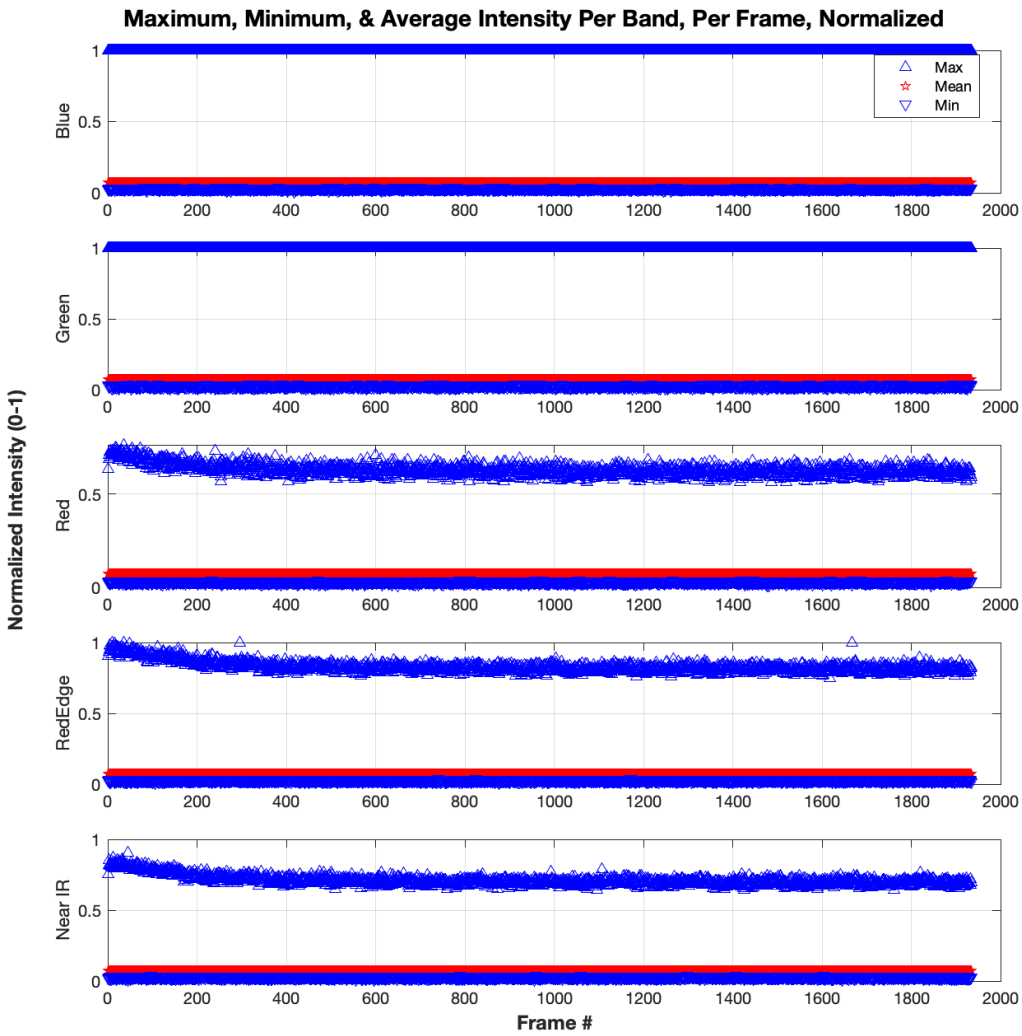

Figure 31. Analysis of Mission 1 images from the MicaSense RedEdge-MX plotting each individual sensors image intensity on a normalized scale from 0 to 1.

The information from this analysis again shows very unusual behavior where both the blue and green band indicate max intensity throughout the entire flight and the red, near infra-red, and red-edge bands all show high levels early in the flight which level off but are still above 0.5 the entire flight.

b. Mission 2 : Flight data shown in Figure 29

The images captured from the Sony UMC-R10C were analyzed for this mission and were processed first by calculating the maximum, minimum, and average change in intensity for the 3,823 RGB images. This was done using the script in the Appendix, Section A, and the graphic is shown in Figure 32.

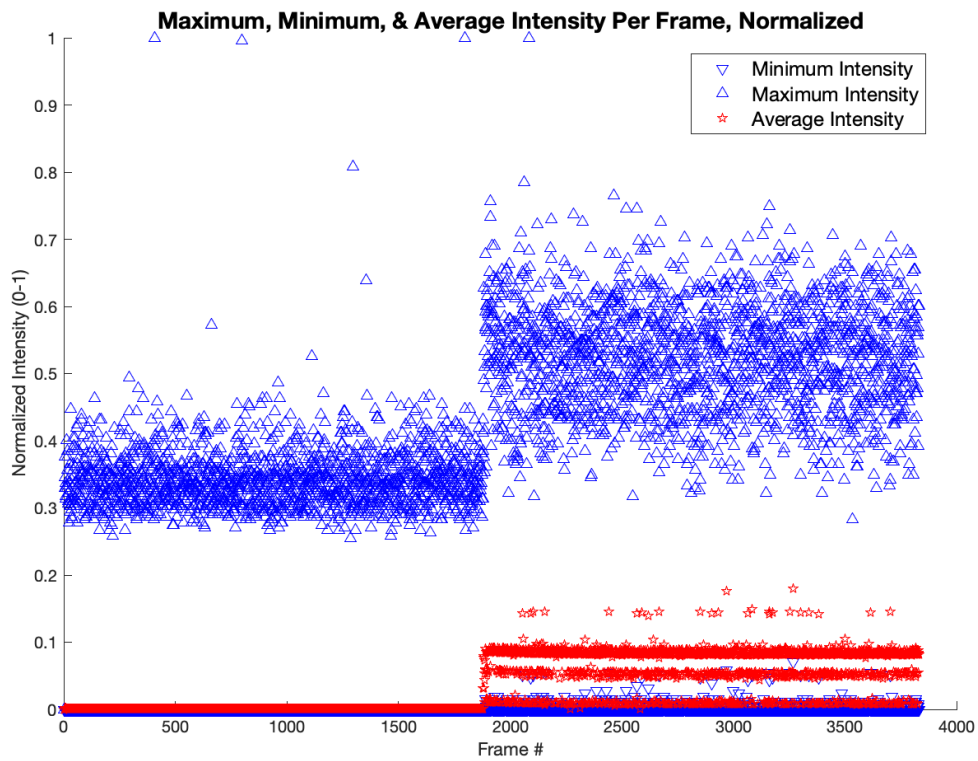

Figure 32. Maximum, minimum, and average change in intensity, normalized, for RGB images captured using the Sony UMC-R10C for Mission 2.

The information shown in Figure 32 is interesting in that it shows minor change in intensity across the first half of images, then a large spike where the average intensity shifts upwards and then another constant state of intensity for the remainder of the flight. An analysis was conducted on images capture from the MicaSense RedEdge-MX for the entire range of photos for all 5 bands using the MATLAB script in the Appendix, Section B, where intensity was plotted on a normalized scale from 0 to 1 and is shown graphically in Figure 33.

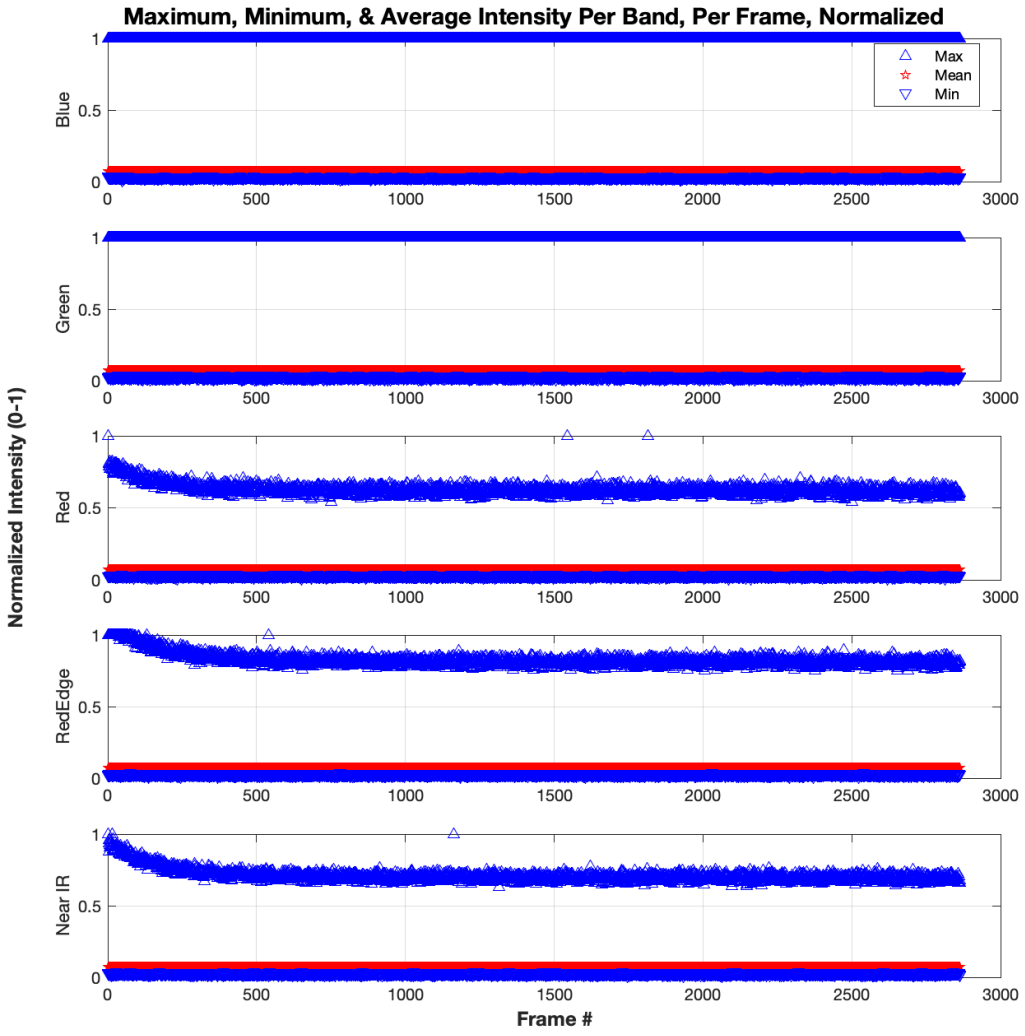

Figure 33. Analysis of Mission 2 images from the MicaSense RedEdge-MX plotting each individual sensors image intensity on a normalized scale from 0 to 1.

Like the MicaSense RedEdge-MX images from Mission 1, these images also show unusual behavior where both the blue and green band indicate max intensity throughout the entire flight and the red, near infra-red, and red-edge bands all show high levels early in the flight which level off but are still above 0.5 the entire flight. A single image from the Sony UMC-R10C was taken and compared against the 5 images captured at the same time stamp from the MicaSense RedEdge-MX and is displayed in Figure 34.

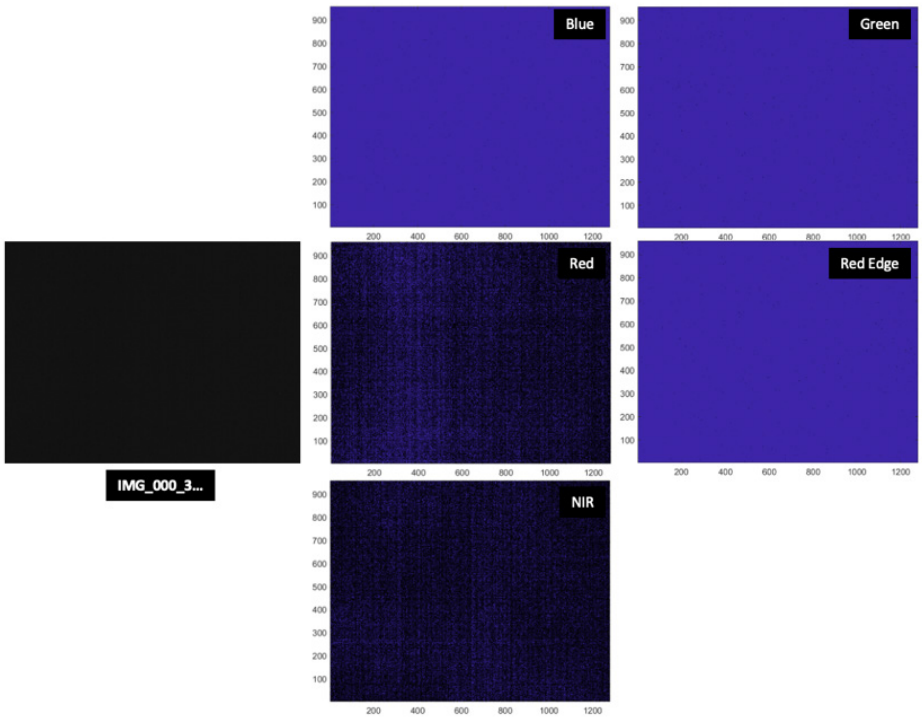

Figure 34. RGB image from the Sony UMC-R10C during Mission 2 alongside five individual bands captured by the MicaSense Red-Edge MX at the same timestamp.

Figure 34 shows the Sony UMC-R10C captured no activity while the blue, green, and red-edge bands of the MicaSense RedEdge-MX are fully saturated, that is all pixels are registering maximum intensity. This indicates a major concern with the image sensing equipment, potentially due to camera configuration.

A final analysis was run on the Sony UMC-10C imagery across the entire range of 3,823 RGB images captured, separating the color channels using the "imsplit" function in the MATLAB Image Processing Toolbox and plotting the color channels fraction of intensity against the frame and is graphically shown in Figure 35.

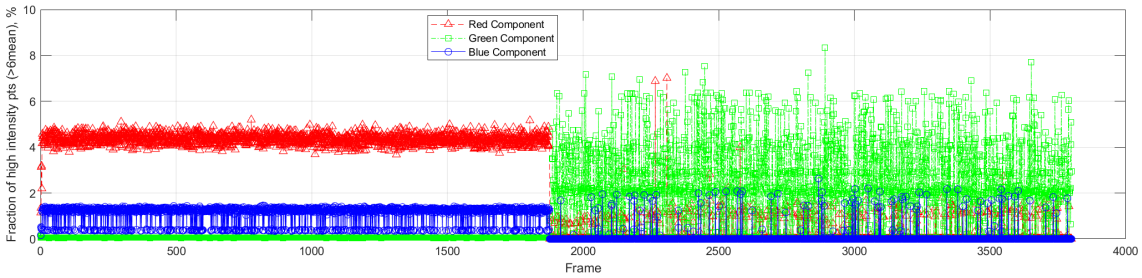

Figure 35. Sony UMC-R10C images processed to show individual color channels fraction of intensity per frame for Mission 2.

Figure 35 depicts a visible shift in the RGB color channel fractional intensity around frame 1900 where red was originally the main fraction component and it shifted dramatically to green. Looking at the flight plan depicted in Figure 29 for mission two there were two search patterns programmed into the same mission, an initial east to west grid over the MBARI AUV, followed by a north to south grid over the same position. Figure 36 shows the Trinity F90+ prior to take off when the anti-collision lights are in place as required for BVLOS night flights per the FAA risk assessment conducted.

Figure 36. Trinity F90+ sUAS with affixed anticollision lighting prior to launch.

The starboard wing of the Trinity F90+ has a green affixed anticollision light and the port wing has a red affixed anticollision light which correlate to the shift of the RGB

color channel fractional intensity which occurred around frame 1,900 when the search pattern shifted direction and most likely had to automate staying on course by keeping a different wing lower. Though this explanation is plausible for the RGB color channel shift in Figure 35 it doesn't fully account for the MicaSense RedEdge-MX color channels having consistent saturation during the entire flight. Figure 37 shows the belly of the Trinity F90+ around the payload compartment while powered on and you can see extensive light pollution from an internal blue light and red light on the payload.

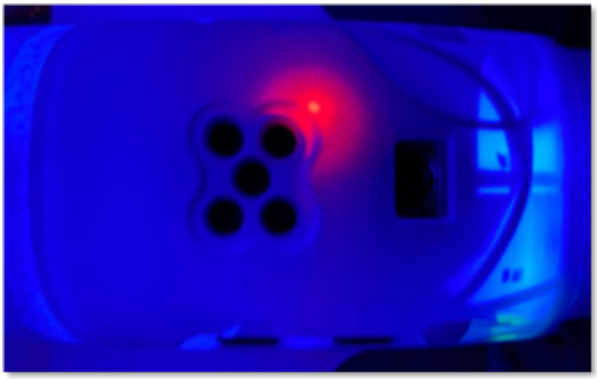

Figure 37. Trinity F90+ payload compartment while powered on showing light pollution from internal blue light and red light on payload.

Though the imagery captured from this experiment in both Mission 1 and 2 did not turn out as intended, much was learned regarding the experimental setup. It is apparent that the Trinity F90+ sUAS creates a substantial amount of light pollution from its factory configuration and must be modified if it is expected to detect low level of bioluminescent light from the ocean at night.

B. LABORATORY TESTING OF SENSORS

From the data analysis in Chapter III, Section A.3, it is apparent that the image sensors utilized by the sUAS were not functioning as intended. A set of laboratory tests were conducted on the payloads for the Trinity F90+ eVTOL sUAS to determine if the sensors could adequately capture low level bioluminescent light and what sensor settings optimized the resulting imagery.

Three sUAS payload sensors were tested. First the MicaSense RedEdge-MX from the dual payload bay in Figure 8b, second, the Sony UMC-R10C 20MP RGB from the same payload, and finally, the Sony RX1-RII 42MP RGB camera which was acquired after the completion of data collection in Chapter II and is shown in Figure 38.

Figure 38. Quantum Systems payload with Sony RXR1-RII payload. Source: [13].

The Sony RXR1-RII payload is the highest quality RGB sensor that Quantum Systems supplies with the Trinity F90+ sUAS and is capable of high analog gain and quick shutter speed. A comparison of the three sensors specifications is shown in Table 1.

Table 1. Trinity F90+ sUAS sensor specifications. Adapted from [13].

	MicaSense RedEdge-MX	Sony UMC-R10C	Sony RX1R II
Spectral Bands	Blue, green, red, red edge, near-IR	RGB	RGB
Dimensions	1,280pix×960pix	5,456pix×3,632pix	7,952pix×5,304pix
Number of Pixels	1,228,800	19,816,192	42,177,408
Field of View	47.1°×36.2°		54.3°×37.8°
Ground Sample Distance	6.7cm per pixel/per band @100m AGL	2.66cm@100m AGL	1.29cm@100m AGL

	MicaSense RedEdge-MX	Sony UMC-R10C	Sony RX1R II
Lens	f=5.5mm	f=16mm, F2.8	f=35mm, F2.0
Trigger Interval	1s (1.4s)	1.1s (1.6s)	1.4s
Weight	380g	429g	694g
Dimensions	9.4cm×6.3cm×4.6cm		
CMOS Sensor Size	4.8mm×3.6mm	23.2mm×15.4mm	35.9mm×24.0mm
Exposure	0.066ms-24.5ms		

The test was set up in a windowless office on the NPS campus to completely remove background light pollution. A light source was placed on a stable surface with an affixed 475nm blue band narrow filter used in Chapter II, Section E.2, approximately 2m (6.5ft) from the sUAS with attached sensor payload. A plastic bottle full of water was placed on top of the light source as a diffuser. Figure 39 is a graphic visualization of the experiment setup.

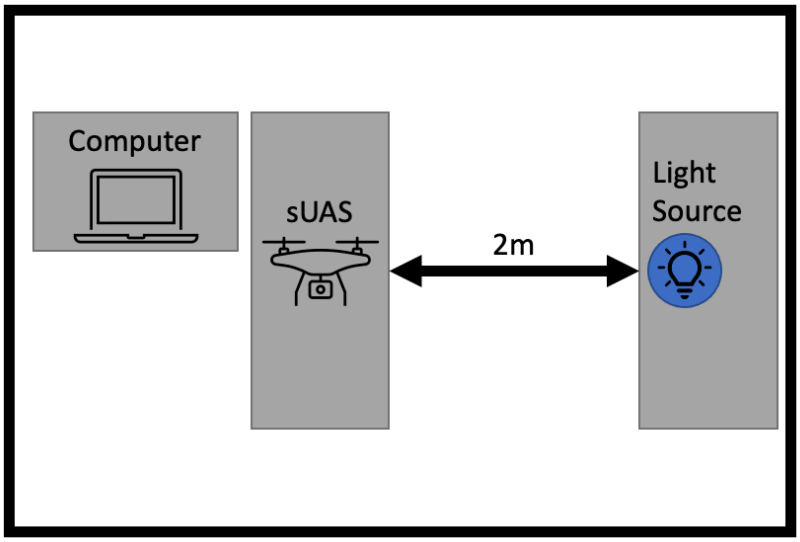

Figure 39. Image sensor testing setup.

From Figure 39, the blue light diffuser was placed on a table top across from the sUAS which had its sensor system facing towards the light source and away from the

computer which was controlling the manual shutter of the sensor. The computer had its brightness turned to minimal level and was used to dial in settings, manually control the sensor shutter, and examine resulting images. The first payload that was tested was the dual MicaSense RedEdge-MX and Sony UMC-R10C which captured images simultaneously from the Quantum Systems mission management software. The default sensor configuration settings for the Sony UMC-R10C did not produce an image and were adjusted to increase the gain and exposure timing. Figure 40a shows the gray scale blue band image from the MicaSense RedEdge-MX and Figure 40b shows the RGB image from the Sony UMC-R10C after the configuration settings were changed.

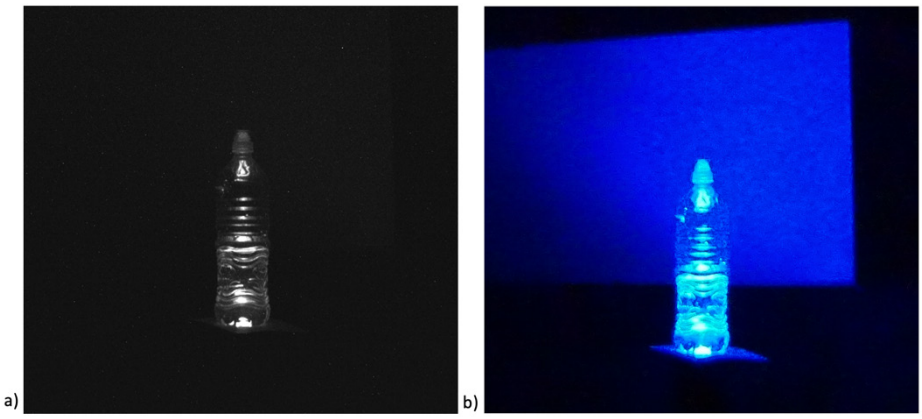

Figure 40. Gray scale blue band image from the MicaSense RedEdge-MX (a) and the RGB image from the Sony UMC-R10C (b).

Both sensors were able to see the diffused blue light in the water bottle clearly while the sUAS was stationary at approximately 2m. The Sony UMC-R10C image was then processed in MATLAB using the "imsplit" function from the Image Processing Toolbox to split the image into its individual color channels and is depicted in Figure 41.

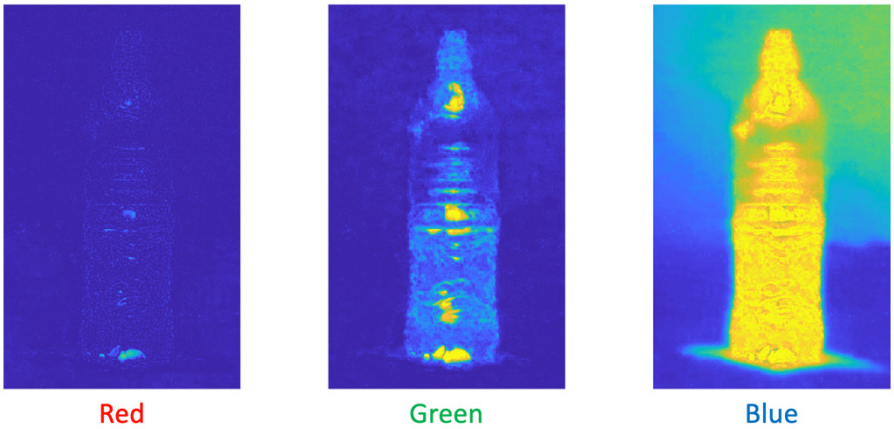

Figure 41. Test image from the Sony UMC-R10C split into three individual, RGB color channels.

From Figure 41 it can be observed that even with the use of the narrow blue band filter on the light diffuser there is still light captured in the green channel and a very small amount in the red channel. This information shows however that the Sony UMC-R10C can detect the narrow band blue light. For the final laboratory analysis of all three sUAS sensors, the test setup from Figure 39 was again set up and each sensor was individual tested using the light source with incremental changes to the emitted light intensity. This was done for each sensor individually, but the incremental changes were the same for each of the sensors going from no light emitted to full light emission of the blue source. Figure 42 shows the combined results of this test using a modification of the MATLAB script in the Appendix, Section A.

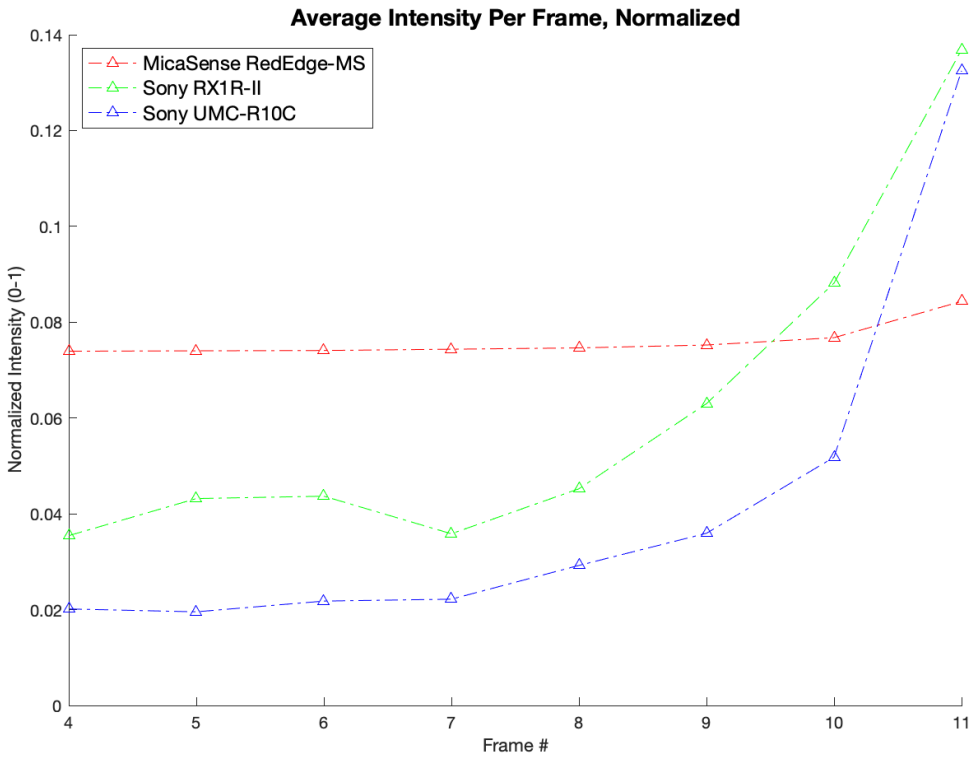

Figure 42. Analysis of image intensity change for each sensor as light intensity was increased incrementally.

Figure 42 reveals that each sensor viewed the incremental changes in a very similar way plotting an exponential increase in the image intensities as it was increased from the light source. The MicaSense RedEdge-MX was the least sensitive to the incremental changes in light, whereas both Sony sensors responded very similarly.

The tests from this section conclude that all three sensors can capture bioluminescent light centering around 475nm in wavelength at varying intensities. The tests also concluded that the sensor default configurations are not satisfactorily tuned for night image capture and the analog gain, shutter speed, and exposure time for each sensor must be optimized for inflight, low altitude, low light capture of bioluminescence. The Sony RX1-RII performed the best in laboratory test environments as it has the highest analog gain setting and pixel ratio in comparison to the Sony UMC-R10C. The Sony UMC-R10C however has a sensor more attuned to low light capture and a faster shutter speed

which are advantageous during flight, and both Sony sensors outperformed the MicaSense RedEdge-MX.

C. JOINT EXPERIMENT 2: SUAS LAUNCHED FROM OFFSHORE VESSEL

The final experiment for this research project was conducted on March 30, 2023, as a cooperative effort between NPS, NOAA, Upwell, and Monterey Bay Whale Watch. This was a follow-up experiment using some of the lessons learned from Joint Experiment 1 to create a second controlled environment for detection of surface and subsurface targets using bioluminescence.

1. Planning Phase

There were two targets for this test, the primary target was the Monterey Whale Watch vessel Pt. Sur Clipper, shown in Figure 43, which is a 55ft single hull passenger vessel with a capacity for 48 persons and the secondary target was any marine mammals sighted during the offshore voyage.

Figure 43. Monterey Bay Whale Watch vessel Pt. Sur Clipper. Source: [27].

During the voyage no marine mammals were encountered thus all the nighttime imagery captured was of the Pt. Sur Clipper while underway in Monterey Bay. The sUAS

used for this experiment was the Upwell owned and NOAA operated DJI Matrice 300 RTK shown in Figure 44.

Figure 44. DJI Matrice 300 RTK rotary sUAS flown by NOAA. Source: [33].

The DJI Matrice 300 RTK is a quad rotary wing sUAS capable of vertical flight and stationary position holding. This sUAS has the advantage over the Trinity F90+ of being able to take off and land from a very small platform as well as hover and track moving targets. The disadvantage of this platform include its flight time in comparison to the fixed wing forward flight of the Trinity F90+ which has a flight time of over 90 minutes, whereas the Matrice 300 has a maximum flight time of 55 minutes if the batteries can hold full capacity [33]. The DJI Matrice 300 was equipped with the MicaSense RedEdge-P multispectral sensor with panchromatic camera shown in Figure 45 and was the most advanced sensor at the time of purchase for the platform.

Figure 45. MicaSense RedEdge-P multispectral sensor plus panchromatic. Source: [34].

This is a substantial improvement over the MicaSense RedEdge-MX since the panchromatic camera gathers intensity data from all 5 individual bands in addition to its own image sensor and is more sensitive to low light.

2. Data Collection

During this experiment a team went offshore with Monterey Bay Whale Watch on the evening of March 30, 2023, with a sunset departure of around 1900. Figure 46 shows the track line of the vessel during the experiment.

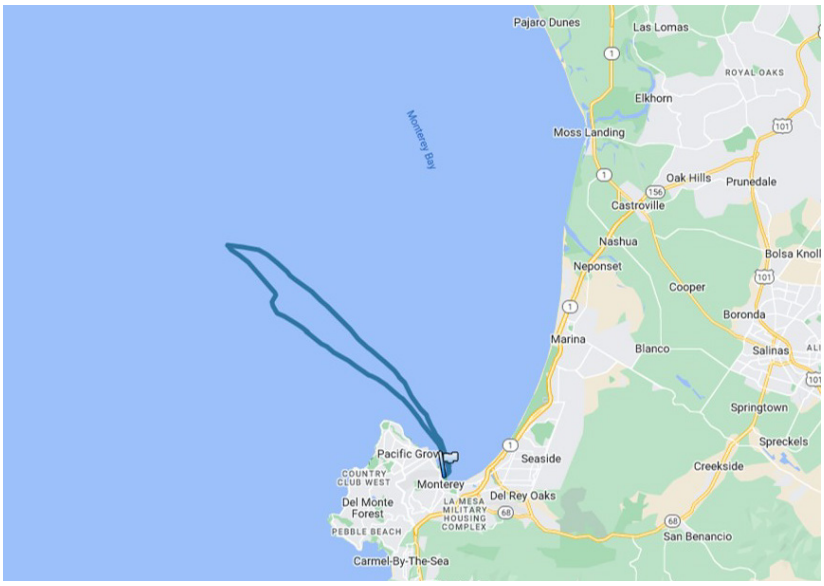

Figure 46. Vessel track line during the March 30, 2023, Joint Experiment 2.

Full darkness was obtained around 2000, and after searching marine mammal hotspots with no sightings the team launched the DJI Matrice 300 RTK from the stern of the vessel and captured imagery of the vessel wake while in motion. Figure 47 shows the team hand launching the sUAS from the stern of the Pt. Sur Clipper.

Figure 47. Team member launching sUAS from the stern of the Pt. Sur Clipper during the March 30, 2023, Joint Experiment 2.

During this experiment 1566 photos were captured by the MicaSense RedEdge-P, 261 per image sensor. As a secondary means of control, the light source used from the image sensor lab experiments in Chapter III, Section B, equipped with the narrow band blue filter was used to create blue light intensity peaks at specific points during the flight to determine if the camera was detecting any levels of lights centered on 475nm.

3. Data Analysis

All data analysis was conducted in MATLAB using the Image Processing Toolbox. The first analysis was done on the blue band sensor images from the MicaSense RedEdge-P using the MATLAB script from the Appendix, Section A, where the maximum, minimum, and average intensities of all 261 photos were calculated and plotted as shown in Figure 48.

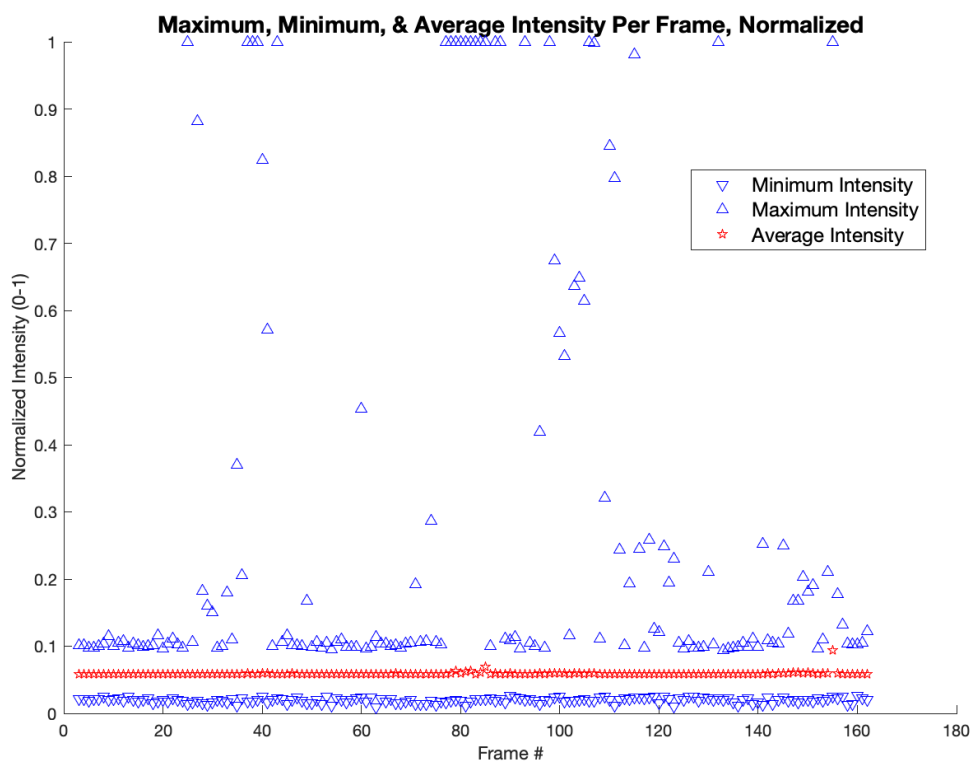

Figure 48. Maximum, minimum, and average change in intensity, normalized, for the blue band centered on 475nm from the MicaSense RedEdge-P during Joint Experiment 2.

From the graph in Figure 48 you can see that there were many maximum intensity spikes in blue light intensity throughout the data capture, but only a few of these spikes occurred in the average change in image intensity. Using this average intensity change, a photo was identified for further processing and is shown in Figure 49a and b.

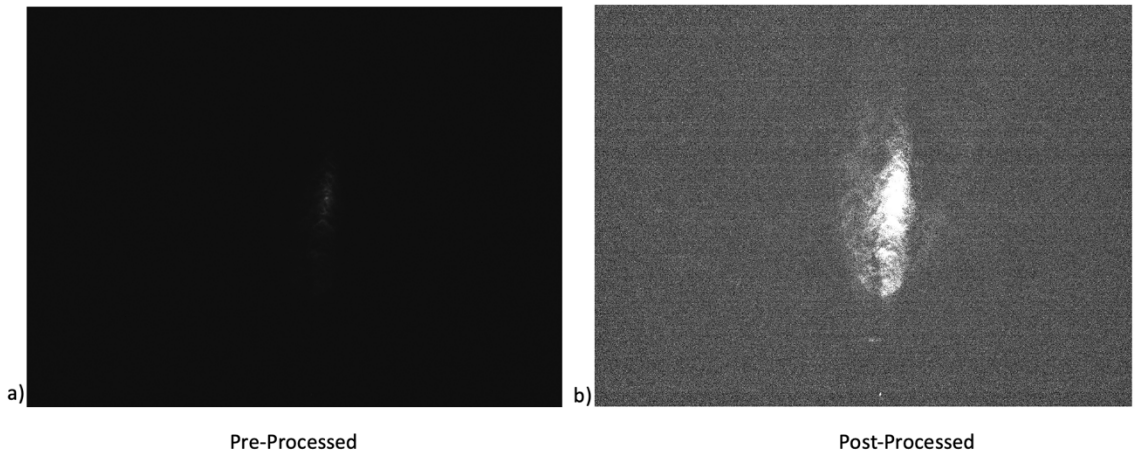

Figure 49. Blue band image before (a) and after (b) adjustment of intensity saturation.

Figure 49a features the original (unprocessed) image, while Figure 49b —the post-processed file using the MATLAB script in the Appendix, Section C.

Specifically, the image processing in Figure 49 conducted an adjustment of the image intensity saturation to only saturate the top 1% and bottom 1% of the image intensity which allows the fine detail of the image to appear. Looking at the pre-processed image in Figure 49a the observer would barely see any blue light captured, but once the processing is done the vessel wake and outline of the light source shining on the vessel wake can clearly be observed. The spikes identified from Figure 48 were moments where the light source was used to illuminate the vessels wake with blue light as a control for bioluminescent light.

The same analysis was conducted on the images captured from the panchromatic sensor using the MATLAB script from the Appendix, Section A to calculate the maximum, minimum, and average change in intensity and is shown in Figure 50.

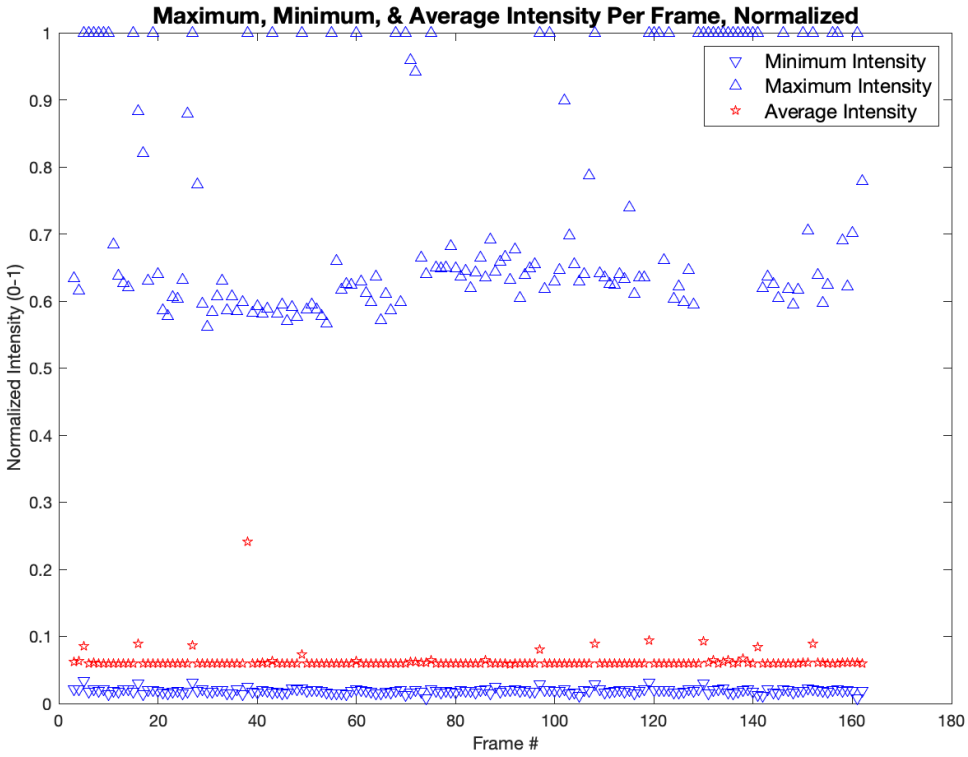

Figure 50. Maximum, minimum, and average change in intensity, normalized, for panchromatic images from the MicaSense RedEdge-P during Joint Experiment 2.

Again, from this graph we can see spikes in average intensity change and a photo was chosen from this set of spikes, which was from the same set of photos used in the blue band analysis and is shown in Figure 49a and b. The panchromatic image was processed using the MATLAB script in the Appendix, Section C to adjust the intensity saturation of this image and bring out the fine detail of the top 1% and bottom 1% of the image intensity and is shown in Figure 51.

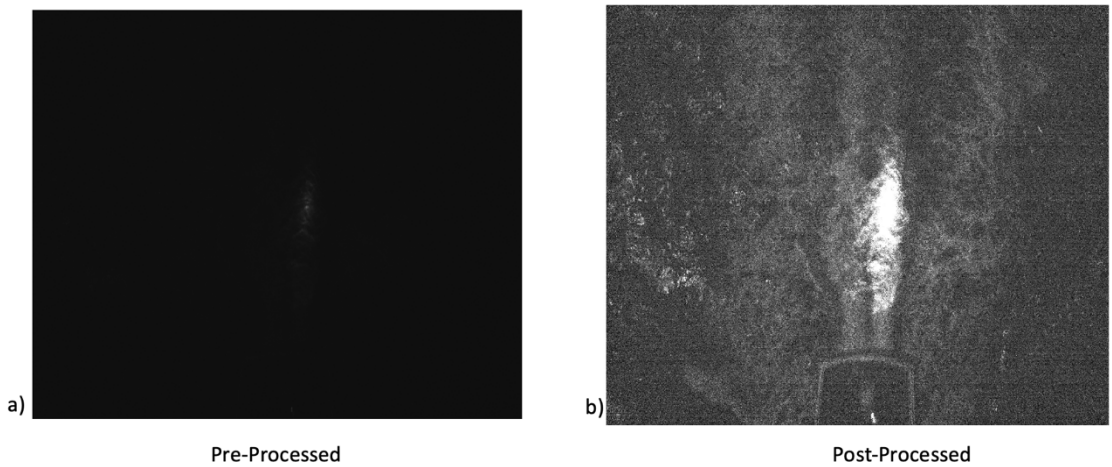

Figure 51. Panchromatic image before (a) and after (b) adjustment of intensity saturation.

This time much more detail is seen from the post processed panchromatic image than from the post processed blue band image of the same series in Figures 49a and b. This difference can be attributed to the panchromatic image sensor being more sensitive to low light and feeding in intensity data from all the 5 other image sensors on the MicaSense RedEdge-P. More of the vessel wake can be seen in Figure 51, well outside the circle of blue from the light source used as a control. To get a better understanding of the amount of intensity data the panchromatic sensor captures another analysis of all 1566 images from the MicaSense RedEdge-P was done using the MATLAB script in the Appendix, Section D, to plot each individual band versus the image intensity which was normalized on a scale from 0–1 and is shown in Figure 52.

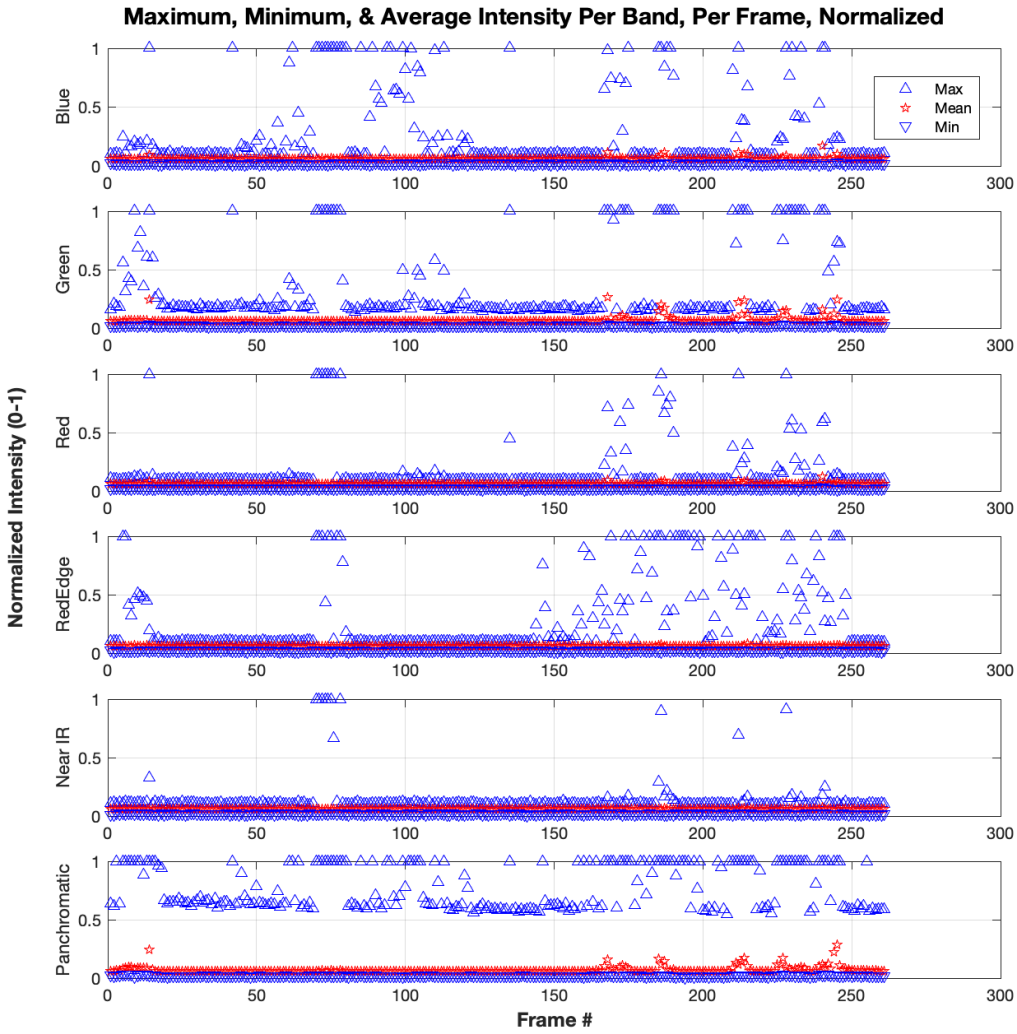

Figure 52. Analysis of all images during Joint Experiment 2 from the MicaSense RedEdge-P plotting each individual sensors image intensity on a normalized scale from 0–1.

Figure 52 clearly shows the panchromatic sensor is much more sensitive to low light than all the other 5 bands since its maximum image intensity stays around 0.5 the entire range of captured images whereas the other bands drop to close to 0 except for where intensity spikes occur. You can also see that the intensity spikes in each band correlate to one another.

IV. CONCLUSION

A. CONCLUSION

This research presented the results of the assessment of an idea of nighttime airborne marine mammal avoidance capability. There were two encompassing areas, flight systems and sensor systems, in which achievements were made and lessons were learned during this project.

1. Flight System

The flight systems utilized during this research include a general aviation aircraft, Trinity F90+ eVTOL sUAS, and DJI Matrice 300 RTK rotary sUAS. A systems approach was used to initially choose the Trinity F90+ as the primary sUAS platform for this research project. The Trinity F90+ can achieve vertical take-off and landing with the energy saving capability of forward fixed wing flight and versatility of easy imaging payload swaps. The Quantum Systems mission management software is intuitive and automates almost all the mission planning process, allowing for the user to have almost no sUAS experience and be able to produce exceptional results. The drawbacks to this system were discovered after initial data collection and include the excessive amount of light pollution produced by the sUAS fuselage near the imaging sensors which polluted captured data. Another main concern with the Trinity F90+ is the inability to adjust the flight plan after a target has been identified, especially since marine mammals are not bound to a search area thus this limits our ability to adapt if a potential sighting was discovered after launch.

After discovery of the lack of mission adaptability of the fixed wing Trinity F90+, NOAA and Upwell volunteered the use of their DJI Matrice 300 RTK which can achieve approximately 55 minutes of flight, track target, and launch from small unstable platforms such as offshore research vessels. This allowed the research team to seek out marine mammal activity without the limitations of fully automated flight plans and to launch relatively quickly once a target was identified. All marine mammal footage captured during this project was captured using a rotary wing sUAS system.

A final lesson learned from the flight systems perspective is that coordination with the FAA takes a lot of time, especially depending upon the flight area, and time of flight. Getting BVLOS approval from the FAA for an offshore night flight was a win for the experiment team and took weeks' worth of effort including the submission of a detailed risk assessment. Had there not already been a COA in place which was easily adapted for use during the BVLOS night operations, the approval from the FAA to conduct this experiment may not have happened.

2. Sensor Systems

Many challenges were identified and overcome during the first phase of data collection. Imagery obtained using a Complementary Metal-Oxide Semiconductor (CMOS) based sensor deployed on a general aviation aircraft showed challenges with both the exposure time creating elongated imagery and the need to filter environmental light to focus the sensor on the specific wavelength needed to detect bioluminescence [10].

The Trinity F90+ sUAS has a plethora of adaptable sensor systems, but choosing a sensor that is capable of nighttime, low intensity, blue light capture while in flight was a challenge since most all the systems are optimized for daytime operations. The preliminary tests using a low-flying small Unmanned Aerial System (sUAS) with affixed Sony UMC-R10C and 5-band MicaSense RedEdge-MX dual payload showed concerns with the percentages of pixels per image based on the altitude of the aircraft dictating a need to reduce experimental altitude to improve the identification of a marine mammal at shallow depth [10].

After the data was analyzed from Joint Experiment 1 in Chapter III, Section A, it was immediately clear that a problem existed with data capture due to the equipment. sUAS light pollution was identified from the Trinity F90+ as well as default sensor configuration issues preventing the exposure time, shutter speed, and gain needed for successful capture of low intensity blue light at night. The laboratory experiments allowed the team to uncover the most optimal conditions for the sUAS systems and sensors to capture quality data at night by adjusting both firmware sensor setting and mission management software settings to collaborate effectively. One major lesson learned was how some sensor systems, such

as the MicaSense sensors, reset after the power is lost, so after every mission and battery change the custom sensor settings must be reset or else it defaults to factory. The mission management software used by Quantum Systems for the Trinity F90+ is great for daylight flight configurations but does not allow advance customization of sensor settings. Getting the custom settings implemented from the sensor company firmware to marry well with the mission control software did not always go as intended and caused some flight data to not save or capture at all.

The use of the MicaSense RedEdge-P on the DJI Matrice 300 RTK was the most optimal flight system and sensor system pair used during this research. The sUAS platform is capable of extended flight time compared to other rotary sUAS systems and when combined with the MicaSense RedEdge-P produce some of the best low light images to date for a COTS system. The DJI Matrice also has a forward-facing built-in camera which allows for the pilot to get live visual sUAS bearing during flight even while flying the MicaSense sensor which does not provide live visual feed back to the controller. This was extremely helpful during sUAS hand catch recovery off the stern of a research vessel at night.

B. FUTURE WORK

This research project took almost two full years of work to get to the point where the research team, flight system, and sensor systems were mature enough to be able to capture marine mammals at night. From the beginning this goal was hard to achieve but the work done by the research team moved the idea several steps forward. Hood Technology is a private research group out of Hood River, Oregon and has partnered with this research team during some of the experiments. They are currently developing an integrated sensor system for the Fire Scout sUAS system with a built-in bioluminescence sensor called PAISO. The results of their work, to include successful capture of marine mammals in bioluminescence at night from a manned general aviation aircraft are included as the first supplemental to this thesis. Working with their team on a custom-built system and using the lessons learned from this research on the capabilities of COTS flight systems and sensors will give the next phase of research a major advantage.

THIS PAGE INTENTIONALLY LEFT BLANK

APPENDIX. MATLAB CODE

All data processing for this experiment was conducted using MATLAB with the Image Processing Toolbox add-on. The code for all the analysis is included in this appendix.

A. CALCULATE AND GRAPH IMAGE INTENSITY

```
% Title – Calculate_Intensity.m
% Authors – LT Justin Goff, Professor Oleg Yakimenko
%
% Notes – This code is used to process image files and calculate the
% maximum, minimum, and average intensity and plot it for a string of
% images. It will normalize the intensity values from 0 to 1.

%% Fresh Start
clearvars; close all; clc;

% Get File Space
d=dir; str={d.name}; S=size(str);

%% Process Tiff Files
% Preallocate Space
kmin = zeros(S);
kmax = zeros(S);
kmean = zeros(S);

% Call Waitbar
h = waitbar(0,'Please wait...');

% Process Files
for f=1:max(S)
  if str{f}(1)~='.' % Ignore '.','..','.DS_Store'
     % Read tiff File
     Ima=imread(str{f});

     % Waitbar Updates
     waitbar(f/max(S));

     % Calculate Maximum, Minimum, & Average Intensity
     kmin(f)=min(Ima(:,:),[],'all');
     kmax(f)=max(Ima(:,:),[],'all');
     kmean(f)=mean(Ima(:,:),'all');
```

```
    % Set Zero values to NaN
    kmin(kmin==0)=NaN;
    kmax(kmax==0)=NaN;
    kmean(kmean==0)=NaN;
  end
end

% Normalize Data from 0 to 1, divide by max(kmax)
nkmax=double(kmax)/max(kmax);
nkmin=double(kmin)/max(kmax);
nkmean=double(kmean)/max(kmax);

% Close Waitbar
close(h)

% Plot kmax, kmin, kmean, normalized yaxis
  set(figure, 'Position',  [350, 200, 700, 500]) %Set Figure Size
  hold
  plot(nkmin,'Vb'), plot(nkmax,'^b'), plot(nkmean,'pr')
  title('Maximum, Minimum, & Average Intensity Per Frame, Normalized', ...
    'FontSize',14)
  ylim([0 1])
  xlabel('Frame #')
  ylabel('Normalized Intensity (0-1)')
  legend('Minimum Intensity','Maximum Intensity','Average Intensity', ...
    'FontSize',12,'location','best')
```

B. PROCESS MICASENSE REDEDGE-MX TIFF IMAGE FILES

```
% Title – Process_TIFF_5Band.m
% Authors – LT Justin Goff, Professor Oleg Yakimenko
%
% Notes – This code is used to process tiff image files collected by
% MicaSense RedEdge-MX sensor or similar with 5 individual bands
% collected and numbered 1 thru 5.

%% Fresh Start
clearvars; close all; clc;

% Get File Space
d=dir; str={d.name}; S=size(str);

%% Process Tiff Files
% Set I
I=1;

% Preallocate Space
```

```
s=sum(count(str,'IMG')==1)/5;
a=zeros(S);
kmaxn=zeros(S);
Trio1=zeros([s,3]);
Trio2=zeros([s,3]);
Trio3=zeros([s,3]);
Trio4=zeros([s,3]);
Trio5=zeros([s,3]);
Trio6=zeros([s,3]);
Fra=zeros([s,5]);

% Call Waitbar
h=waitbar(0,'Please wait...');

% Process Files
for f=1:max(S)
 if str{f}(1)~='.' % Ignore '.','..','.DS_Store'
    % Read tiff File
    Ima=imread(str{f});
    band=str2double(str{f}(10));

    % Waitbar Updates
    waitbar(f/max(S));

    % Calculate Maximum, Minimum, & Average Intensity
    kmaxn(f)=max(Ima(:,:),[],'all');
    kmax=max(Ima(:,:),[],'all');
    kmean=mean(Ima(:,:),'all');
    kmin=min(Ima(:,:),[],'all');

    % Set Zero values to NaN
    kmin(kmin==0)=NaN;
    kmax(kmax==0)=NaN;
    kmean(kmean==0)=NaN;

    % Split into bands
    a(band)=length(find(Ima(:,:)>6*kmean));
    switch band
       case 1, Trio1(I,:)=double([kmax kmean kmin]);
       case 2, Trio2(I,:)=double([kmax kmean kmin]);
       case 3, Trio3(I,:)=double([kmax kmean kmin]);
       case 4, Trio4(I,:)=double([kmax kmean kmin]);
       case 5, Trio5(I,:)=double([kmax kmean kmin]);
       Fra(I,:)=[a(1) a(2) a(3) a(4) a(5)]/(numel(Ima))*100;
       I=I+1;
    end
 end
```

```
end

% Normalize Data from 0 to 1, divide by max(kmax)
Trio1=Trio1/max(kmaxn);
Trio2=Trio2/max(kmaxn);
Trio3=Trio3/max(kmaxn);
Trio4=Trio4/max(kmaxn);
Trio5=Trio5/max(kmaxn);

% Close Waitbar
close(h)

%% 5 Band Subplot
set(figure,'Position',[350, 200, 700, 700]) %Set Figure Size
hold
rnge=1:length(Trio1);
subplot(5,1,1), plot(rnge,Trio1(:,1),'^b',rnge,Trio1(:,2),'pr',rnge,Trio1(:,3),'Vb')
ylabel('Blue'), grid, yticks([0 0.5 1]), yticklabels([0 0.5 1])
sgtitle('Maximum, Minimum, & Average Intensity Per Band, Per Frame, Normalized', ...
    'FontSize',14,'FontWeight','Bold')
legend('Max','Mean','Min','location','best')
subplot(5,1,2), plot(rnge,Trio2(:,1),'^b',rnge,Trio2(:,2),'pr',rnge,Trio2(:,3),'Vb')
ylabel('Green'), grid, yticks([0 0.5 1]), yticklabels([0 0.5 1])
subplot(5,1,3), plot(rnge,Trio3(:,1),'^b',rnge,Trio3(:,2),'pr',rnge,Trio3(:,3),'Vb')
ylabel('Red'), grid, yticks([0 0.5 1]), yticklabels([0 0.5 1])
subplot(5,1,4), plot(rnge,Trio4(:,1),'^b',rnge,Trio4(:,2),'pr',rnge,Trio4(:,3),'Vb')
ylabel('RedEdge'), grid, yticks([0 0.5 1]), yticklabels([0 0.5 1])
subplot(5,1,5), plot(rnge,Trio5(:,1),'^b',rnge,Trio5(:,2),'pr',rnge,Trio5(:,3),'Vb')
ylabel('Near IR'), grid, yticks([0 0.5 1]), yticklabels([0 0.5 1])
xlabel('Frame #','FontSize',12,'FontWeight','Bold')
[ax,h1]=suplabel('Normalized Intensity (0-1)','y'); %Suplabel Add-On
set(h1,'FontSize',12,'FontWeight','Bold')
```

C. ADJUST IMAGE INTENSITY SATURATION

```
% Title – Imadjust_tiff2png.m
% Authors – LT Justin Goff
%
% Notes – This code is used to process tiff image files using the
% imadjust function to saturate only the top 1% and bottom 1% of image
% saturation to better see the fine details and save file as PNG.

%% Fresh Start
clearvars; close all; clc;

% Get File Space
d=dir; str={d.name}; S=size(str);
```

```
% Turn off figure visibility
set(0,'DefaultFigureVisible','off');

%% Process Tiff Files

% Call Waitbar
h = waitbar(0,'Please wait...');

% Process Files
for f=1:10 %max(S)
  if str{f}(1)~='.' % Ignore '.','..','.DS_Store'
      % Read tiff File
      Ima=imread(str{f});

      % Waitbar Updates
      waitbar(f/max(S));

      % Display Original and Save Figure
      ia=imadjust(Ima);
      imshow(ia)
      saveas(gcf,sprintf(str{f}(1:end-4)),'png')
      close

      % Reset Workspace for Next Folder
      clear i ia file
  end
end

% Close Waitbar
close(h)

% Turn on figure visibility
set(0,'DefaultFigureVisible','on');
```

D. PROCESS MICASENSE REDEDGE-P TIFF IMAGE FILES

```
% Title – Process_TIFF_6Band.m
% Authors – LT Justin Goff, Professor Oleg Yakimenko
%
% Notes – This code is used to process tiff image files collected by
% MicaSense RedEdge-P sensors or similar with 6 individual bands
% collected and numbered 1 thru 6.

%% Fresh Start
clearvars; close all; clc;
```

```
% Get File Space
d=dir; str={d.name}; S=size(str);

%% Process Tiff Files
% Set I
I=1;

% Preallocate Space
s=sum(count(str,'IMG')==1)/6;
a=zeros(S);
kmaxn=zeros(S);
Trio1=zeros([s,3]);
Trio2=zeros([s,3]);
Trio3=zeros([s,3]);
Trio4=zeros([s,3]);
Trio5=zeros([s,3]);
Trio6=zeros([s,3]);
Fra=zeros([s,6]);

% Call Waitbar
h=waitbar(0,'Please wait...');

% Process Files
for f=1:max(S)
 if str{f}(1)~='.' % Ignore '.','..','.DS_Store'
    % Read tiff File
    Ima=imread(str{f});
    band=str2double(str{f}(10));

    % Waitbar Updates
    waitbar(f/max(S));

    % Calculate Maximum, Minimum, & Average Intensity
    kmaxn(f)=max(Ima(:,:),[],'all');
    kmax=max(Ima(:,:),[],'all');
    kmean=mean(Ima(:,:),'all');
    kmin=min(Ima(:,:),[],'all');

    % Set Zero values to NaN
    kmin(kmin==0)=NaN;
    kmax(kmax==0)=NaN;
    kmean(kmean==0)=NaN;

    % Split into bands
    a(band)=length(find(Ima(:,:)>6*kmean));
    switch band
       case 1, Trio1(I,:)=double([kmax kmean kmin]);
```

```
        case 2, Trio2(I,:)=double([kmax kmean kmin]);
        case 3, Trio3(I,:)=double([kmax kmean kmin]);
        case 4, Trio4(I,:)=double([kmax kmean kmin]);
        case 5, Trio5(I,:)=double([kmax kmean kmin]);
        case 6, Trio6(I,:)=double([kmax kmean kmin]);
        Fra(I,:)=[a(1) a(2) a(3) a(4) a(5) a(6)]/(numel(Ima))*100;
        I=I+1;
    end
  end
end

% Normalize Data from 0 to 1, divide by max(kmax)
Trio1=Trio1/max(kmaxn);
Trio2=Trio2/max(kmaxn);
Trio3=Trio3/max(kmaxn);
Trio4=Trio4/max(kmaxn);
Trio5=Trio5/max(kmaxn);
Trio6=Trio6/max(kmaxn);

% Close Waitbar
close(h)

%% 6 Band Subplot
set(figure,'Position',[350, 200, 700, 700]) %Set Figure Size
hold
rnge=1:length(Trio1);
subplot(6,1,1), plot(rnge,Trio1(:,1),'^b',rnge,Trio1(:,2),'pr',rnge,Trio1(:,3),'Vb')
ylabel('Blue'), grid
sgtitle('Maximum, Minimum, & Average Intensity Per Band, Per Frame, Normalized', ...
    'FontSize',14,'FontWeight','Bold')
legend('Max','Mean','Min','location','best')
subplot(6,1,2), plot(rnge,Trio2(:,1),'^b',rnge,Trio2(:,2),'pr',rnge,Trio2(:,3),'Vb')
ylabel('Green'), grid
subplot(6,1,3), plot(rnge,Trio3(:,1),'^b',rnge,Trio3(:,2),'pr',rnge,Trio3(:,3),'Vb')
ylabel('Red'), grid
subplot(6,1,4), plot(rnge,Trio4(:,1),'^b',rnge,Trio4(:,2),'pr',rnge,Trio4(:,3),'Vb')
ylabel('RedEdge'), grid
subplot(6,1,5), plot(rnge,Trio5(:,1),'^b',rnge,Trio5(:,2),'pr',rnge,Trio5(:,3),'Vb')
ylabel('Near IR'), grid
subplot(6,1,6), plot(rnge,Trio6(:,1),'^b',rnge,Trio6(:,2),'pr',rnge,Trio6(:,3),'Vb')
ylabel('Panchromatic'), grid
xlabel('Frame #','FontSize',12,'FontWeight','Bold')
[ax,h1]=suplabel('Normalized Intensity (0-1)','y'); %Suplabel Add-On
set(h1,'FontSize',12,'FontWeight','Bold')
```

E. MP4 VIDEO PROCESSING

```
% Title – Video_Processing.m
% Authors – LT Justin Goff, Professor Oleg Yakimenko
%
% Notes – This code is used to process .MP4 files and calculate the
% maximum, minimum and average intensity and plot it for a string of
% frames. It will normalize the intensity values from 0 to 1. The
% latter two sections of code with conduct a single frame enhancement
% using the imadjust function and layer subtraction. Update line 70 to
% include video frame # for processing.

%% Fresh Start
clearvars; close all; clc;

% Import .MP4 file
v=VideoReader("Summary_Brief_3.mp4");

%% Process .MP4 Files
% Preallocate Space
kmin=NaN([1,v.NumFrames]);
kmax=NaN([1,v.NumFrames]);
kmean=NaN([1,v.NumFrames]);

% Call Waitbar
h = waitbar(0,'Please wait...');

% Process Frames
for f=1:v.NumFrames
  vidFrame = readFrame(v);

  % Waitbar Updates
  waitbar(f/v.NumFrames);

  % Calculate Maximum, Minimum, & Average Intensity
  kmin(f)=min(vidFrame(:,:,:),[],'all');
  kmax(f)=max(vidFrame(:,:,:),[],'all');
  kmean(f)=mean(vidFrame(:,:,:),'all');

  % Set Zero values to NaN
  kmin(kmin==0)=NaN;
end

% Normalize Data from 0 to 1, divide by max(kmax)
nkmax=double(kmax)/max(kmax);
nkmin=double(kmin)/max(kmax);
nkmean=double(kmean)/max(kmax);
```

```
% Close Waitbar
close(h)

%% Plot Intensity Data
% Plot kmax, kmin, kmean, normalized yaxis
set(figure, 'Position',  [350, 200, 900, 700]) %Set Figure Size
hold
plot(nkmin,'Vb'), plot(nkmax,'^b'), plot(nkmean,'pr')

% Identify Intensity Spikes
nkstd=std(nkmean);
lll=find(diff(nkmean)>nkstd);
stem(lll,50*ones(size(lll)))

% Figure Options
title('Maximum, Minimum, & Average Intensity Per Frame, Normalized', ...
  'FontSize',14)
ylim([0 1])
xlabel('Frame #')
ylabel('Normalized Intensity (0-1)')
legend('Minimum Intensity','Maximum Intensity','Average Intensity', ...
  'Intensity Change > Stdev','FontSize',12,'location','best')

%% Display High Intensity Image
vidFrame = read(v,6500); %update to include desired frame for processing.
tiledlayout(1,2)

  %Tile1
  nexttile
  imshow(vidFrame(:,:,3));

  %Tile2
  nexttile
  %Plot Single Frame Grayscale with Saturation Adjustment
  Ig=im2gray(vidFrame(:,:,3));
  J=imadjust(Ig);
  imshow(J)

%Figure Size
set(gcf, 'Position',  [500, 500, 1800, 600]) %Set Figure Size

%%
figure
tiledlayout(1,2);

  %Tile1
```

```
  nexttile
  imagesc(vidFrame(:,:,3));

  %Tile2
  nexttile
  Y=10;
  mesh(vidFrame(end-10:-1:10,Y:end-Y,3));

%Figure Size
set(gcf, 'Position',  [500, 500, 1800, 600]) %Set Figure Size
```

SUPPLEMENTALS

A. SUPPLEMENTAL 1: PRESENTATION OF HOODTECH RESEARCH RESULTS

An email (A. Flotow, email, Apr. 2023) containing this presentation is from Hood Technology Corporation in Hood River, Oregon on their research results as part of a parallel research effort to this thesis. HoodTech conducted a shallow search of a 10-mile swath of ocean using a ship-based UAS in October 2022 with confirmed marine mammal footage in bioluminescent waters. This report was created by Dr. Andreas von Flotow (HoodTech), Rear Admiral Tom Q. Donaldson (USN retired) and Dr. Shaju John (HoodTech).

B. SUPPLEMENTAL 2: CLASSIFIED ANALYSIS OF ASW SUMMARY BRIEF VIDEO FILES. THIS ANALYSIS IS CLASSIFIED SECRET.

This analysis was conducted on classified video footage from the results of USN ASW exercises. This analysis is classified SECRET.

C. SUPPLEMENTAL 3: PRESENTATION OF NON-ACOUSTIC ASW OVERVIEW. THIS PRESENTATION IS CLASSIFIED SECRET//NOFORN.

A SIPR email (R. D. Brodie CDR USN, email, Nov. 2021) containing this presentation for the USN by Dynamic Technologies Inc, with background information on non-acoustic ASW. This presentation is classified SECRET//NOFORN.

D. SUPPLEMENTAL 4: VIDEO SUMMARY OF ASW EXERCISE RESULTS AND BIOLUMINESCENCE RESEARCH. THIS VIDEO IS CLASSIFIED SECRET.

A SIPR email (R. D. Brodie CDR USN, email, Nov. 2021) containing this video summary with footage from the results of USN ASW exercises. This video is classified SECRET.

THIS PAGE INTENTIONALLY LEFT BLANK

LIST OF REFERENCES

[1] UNCTAD Stat, "Merchant fleet by flag of registration and by type of ship, annual." Accessed: Mar. 06, 2023 [Online]. Available: https://unctadstat.unctad.org/wds/TableViewer/tableView.aspx?ReportId=93

[2] K. Hunt, "Blue whales end up as 'ocean's roadkill' in the crowded waters of Patagonia," *CNN*, Jul. 15, 2022 [Online]. Available: https://www.cnn.com/2022/07/15/americas/whales-ships-collisions-patagonia-scn/index.html

[3] R. P. Schoeman, C. Patterson-Abrolat, and S. Plön, "A global review of vessel collisions with marine animals," *Front. Mar. Sci.*, vol. 7, May 2020 [Online]. Available: https://doi.org/10.3389/fmars.2020.00292

[4] E. Cheung, J. Mees, and W. Ripley, "In the dark depths of the Pacific, U.S. submarines patrol with an eye fixed firmly on China," *CNN*, Apr. 06, 2023 [Online]. Available: https://www.cnn.com/2023/04/05/us/us-navy-submarine-pacific-china-intl-hnk-ml/index.html

[5] B. Werner, "USCGC Munro returns from patrol with record cocaine haul," Jul. 11, 2019 [Online]. Available: https://news.usni.org/2019/07/11/uscgc-munro-returns-from-patrol-with-record-cocaine-haul

[6] International Whaling Commission, "Ship strikes," Aug. 18, 2022 [Online]. Available: https://iwc.int/management-and-conservation/ship-strikes

[7] L. Bedriñana-Romano *et al.*, "Defining priority areas for blue whale conservation and investigating overlap with vessel traffic in Chilean Patagonia, using a fast-fitting movement model," *Sci. Rep.*, vol. 11, no. 1, p. 2709, Feb. 2021.

[8] R. Brodie and T. Q. Donaldson, "Use bioluminescence to own the ASW night," *Proceeings*, vol. 147/10/1,424, Oct. 2021 [Online]. Available: https://www.usni.org/magazines/proceedings/2021/october/use-bioluminescence-own-asw-night

[9] J. S. Schoonmaker, Y. Podobna, C. D. Boucher, D. R. Statter, and V. M. Contarino, "Electro-optical approach for airborne marine mammal surveys and density estimations," Oct. 2011 [Online]. Available: https://apps.dtic.mil/sti/citations/ADA585667

[10] J. Goff, A. Elbrecht, and O. Yakimenko, "Challenges in developing nighttime airborne marine mammal avoidance capability," in *OCEANS 2022, Hampton Roads*, Oct. 2022 [Online]. Available: https://ieeexplore.ieee.org/document/9977068

[11] M. Valiadi and D. Iglesias-Rodriguez, "Understanding bioluminescence in dinoflagellates—How far have we come?," *Microorganisms*, vol. 1, no. 1, pp. 3–25, Sep. 2013.

[12] I. Gomez and C. Zdanowicz, "Bioluminescent waves light up Big Sur. And what a sight it is," *CNN*, Feb. 07, 2018 [Online]. Available: https://www.cnn.com/2018/02/07/us/big-sur-bioluminescent-waves-trnd/index.html

[13] Quantum-Systems, "Trinity F90+ payloads," May 14, 2022 [Online]. Available: https://www.quantum-systems.com/project/trinity-f90plus-payloads/

[14] MicaSense, "What is the center wavelength and bandwidth of each filter for MicaSense sensors?," Oct. 21, 2022 [Online]. Available: https://support.micasense.com/hc/en-us/articles/214878778-What-is-the-center-wavelength-and-bandwidth-of-each-filter-for-MicaSense-sensors

[15] MicaSense, "Dual camera imaging system," Oct. 17, 2019 [Online]. Available: https://micasense.com/dual-camera-system/

[16] Diffraction Limited, "SBIG STC-428-OEM – Astronomy & scientific imaging solutions," May 14, 2022 [Online]. Available: https://diffractionlimited.com/product/stc-428-oem/

[17] Nikon Inc., "Nikon AF-S NIKKOR 50mm f/1.8G lens," May 14, 2022 [Online]. Available: https://www.nikonusa.com/en/nikon-products/product/camera-lenses/af-s-nikkor-50mm-f%252f1.8g.html

[18] Midwest Optical Systems, "Bandpass filters." Accessed: May 14, 2022 [Online]. Available: https://midopt.com/filters/bandpass/

[19] Quantum-Systems, "Discover Trinity F90+- the unbeatable mapping drone," Jan. 23, 2023 [Online]. Available: https://quantum-systems.com/trinity-f90/

[20] Quantum-Systems, "Sony UMC-R10C," Aug. 18, 2022 [Online]. Available: https://www.quantum-systems.com/project/sony-umc-r10c/

[21] U.S. Coast Guard, "United States Coast Guard." Accessed: May 01, 2023 [Online]. Available: https://www.uscg.mil/

[22] MBARI, "Homepage • MBARI." Accessed: May 01, 2023 [Online]. Available: https://www.mbari.org/

[23] Insight Up Solutions, "Insight Up Solutions | Commercial drone technologies and software solutions." Accessed: May 01, 2023 [Online]. Available: https://insightupsolutions.com/

[24] Naval Postgraduate School, “Naval Postgraduate School.” Accessed: May 01, 2023 [Online]. Available: https://nps.edu/

[25] National Oceanic and Atmospheric Administration, “National Oceanic and Atmospheric Administration.” Accessed: May 01, 2023 [Online]. Available: https://www.noaa.gov/

[26] Naval Research Lab, “NRL.” Accessed: May 01, 2023 [Online]. Available: https://www.nrl.navy.mil/marine-meteorology/

[27] Monterey Bay Whale Watch, “Monterey Bay Whale Watch – Whale watching trips.” Accessed: May 01, 2023 [Online]. Available: https://montereybaywhalewatch.com/

[28] Upwell, “Upwell.” Accessed: May 01, 2023 [Online]. Available: https://www.upwell.org

[29] MBARI, “Vehicles.” Accessed: May 01, 2023 [Online]. Available: https://www.mbari.org/our-work/technologies/vehicles/

[30] “AUV dashboard.” MBARI Pontus. Accessed: May 01, 2023 [Online]. Available: https://okeanids.mbari.org/dash4/#/-/*pontus

[31] “2022 phases of the Moon.” Griffith Observatory Foundation. Accessed: Jun. 06, 2022 [Online]. Available: https://griffithobservatory.org/explore/observing-the-sky/whats-in-the-sky/the-moon/2022-phases-of-the-moon/

[32] U.S. Coast Guard, “About U.S. Coast Guard assets.” Accessed: May 01, 2023 [Online]. Available: https://www.uscg.mil/About/Assets/

[33] DJI, “Matrice 300 RTK – Built tough. Works smart.” Accessed: May 02, 2023 [Online]. Available: https://enterprise.dji.com/matrice-300

[34] Quantum-Systems, “MicaSense RedEdge-P – Quantum-Systems GmbH,” Jan. 24, 2023 [Online]. Available: https://quantum-systems.com/micasense-rededge-p/

THIS PAGE INTENTIONALLY LEFT BLANK

INITIAL DISTRIBUTION LIST

1. Defense Technical Information Center
   Ft. Belvoir, Virginia

2. Dudley Knox Library
   Naval Postgraduate School
   Monterey, California

DUDLEY KNOX LIBRARY

NAVAL POSTGRADUATE SCHOOL

WWW.NPS.EDU

WHERE SCIENCE MEETS THE ART OF WARFARE